Materials Today Bio 32 (2025) 101734

Contents lists available at ScienceDirect

Materials Today Bio

journal homepage: www.journals.elsevier.com/materials-today-bio

Development of a decellularized extracellular matrix-derived wet adhesive for sustained drug delivery and enhanced wound healing

Xinming Wang *, Haonan Zhang, Weichang Xie, Bei Qian, Shixing Huang, Qiang Zhao **, Xiaofeng Ye ***

Department of Cardiovascular Surgery, Ruijin Hospital, Shanghai Jiaotong University School of Medicine, Shanghai, China

ARTICLE INFO

Keywords:
Wet adhesion
Extracellular matrix derived-material
Drug delivery
Volumetric muscle loss
Wound healing

ABSTRACT

Complete tissue recovery following traumatic injury remains a major clinical challenge. While tissue adhesives show promise for managing traumatic injuries, developing materials with robust wet adhesion and high biocompatibility remains difficult. Decellularized extracellular matrix (ECM)-derived materials are widely utilized in tissue engineering due to their superior biocompatibility and bioactivity. In this study, a wet adhesive is developed by functionalizing ECM with dopamine. The resulting ECM-dopamine exhibits strong wet adhesion and excellent biocompatibility. Furthermore, ECM-dopamine can be engineered into a drug delivery platform for small agents and macromolecules. Solid lipid nanoparticles (SLNs) are incorporated into ECM-dopamine to enable sustained release of small molecules. The ECM-dopamine-SLN system ensures sustained drug release for at least one week upon adhesion to target tissues. ECM-dopamine-SLN loaded with antimicrobials accelerates wound healing and promotes angiogenesis by modulating the inflammatory response in a mouse skin excision model. Additionally, ECM-dopamine can deliver bioactive macromolecules to injured tissue. ECM-dopamine loaded with insulin-like growth factor-1 promotes skeletal muscle regeneration in a mouse volumetric muscle loss model, likely through the modulation of M2-like macrophage polarization. The dual functionality of ECM-dopamine as both a wet adhesive and a drug delivery platform offers significant potential for regenerative medicine applications.

1. Introduction

Traumatic wounds are among the most common reasons for patient visits to the Emergency Department [1]. Penetrating wounds, a severe form of traumatic injury, often result in extensive damage to the skin, muscle, and bone. A significant proportion of patients with penetrating wounds, such as gunshot victims, can be stabilized through the use of wound-closing agents to prevent blood loss [2]. However, complete recovery after surgical repair is often hindered by tissue loss, infection, and inflammation. While antimicrobial agents can help mitigate infection, the regeneration of lost tissue, particularly muscle, remains a significant challenge. Various biomaterials and medical devices have been developed to enhance tissue repair following traumatic injuries [3]. Despite these advancements, no effective therapy currently exists to fully reverse the damage. Tissue adhesives with controlled drug delivery capabilities present a promising approach for addressing the complex challenges associated with traumatic wound treatment.

Developing reliable water-resistant adhesives remains a key challenge in wet adhesive research. In aqueous environments, water molecules form a hydration layer on material surface, interfering with molecular bonding between the substrate and the adhesive. [4]. Additionally, the infiltration of water molecules into the adhesive can alter its physical and chemical properties, which eventually leads to cohesive failure [5]. Bio-inspired materials have provided potential solutions for the wet adhesion problem. Certain marine organisms, like mussels, can firmly attach to foreign substrates in seawater. Mussels adhere to the wet surface through secreted mussel foot proteins which contain adhesive residues such as 3,4-dihydroxy-l-phenylalanine (DOPA) and charged groups [6–9]. DOPA is regarded as the most important adhesive primer in mussel foot proteins [10]. DOPA mediates various interactions between mussel foot proteins and substrate surface, including bidentate hydrogen bond, metal-catechol coordination bond, oxidative

* Corresponding author.
** Corresponding author.
*** Corresponding author.
E-mail address: wangxinming2022@sjtu.edu.cn (X. Wang).

https://doi.org/10.1016/j.mtbio.2025.101734
Received 14 February 2025; Received in revised form 28 March 2025; Accepted 5 April 2025
Available online 5 April 2025

crosslinking, and electrostatic forces [11]. In practical applications, DOPA can be utilized as an adhesive agent for distinct substrates, such as silica, metal, and organic film [12]. The robust interfacial chemistry of DOPA provides a unique tool for designing biological adhesives. Many DOPA-functionalized polymers and hydrogels have been developed [13]. However, most of these materials are limited to topical applications due to biosafety concerns.

Decellularized extracellular matrix (ECM) is a biomaterial derived from natural tissue. ECM exhibits high biocompatibility and, more importantly, bioactivity. ECM hydrogels can direct cell differentiation and stimulate cell proliferation due to their inherent growth factors [14–17]. *In vivo* studies have demonstrated that ECM materials are potential therapeutics for organ injuries, such as myocardial infarction and hepatic fibrosis [18–20]. Additionally, ECM hydrogels can serve as injectable drug delivery platforms for cardiac diseases [21]. Although ECM is a promising material for regenerative medicine, current ECM faces several limitations, including rapid degradation, low mechanical strength, and restricted delivery methods. For instance, cardiac ECM hydrogels administrated via intramyocardial injection remain in the heart for approximately 7 days, which is significantly shorter than the 3-week-long post-injury response following myocardial infarction [22]. Further optimizations are necessary to produce ECM-based therapeutics for clinical applications.

Increase the retention of therapeutic agents within target organs is one of the major challenges in the development of drug delivery platforms. Maintaining a relatively high concentration of drugs at the target site not only improves therapeutic efficacy but also minimizes the risk of systemic adverse effects. Currently, a majority of bioactive macromolecules, including mRNA and growth factors, are administrated via injection [23]. Maintaining therapeutic levels of these bioactive molecules requires repeated injections, which can be painful and inconvenient for patients. In certain cases, such as intramyocardial administration, repeated injections significantly increase the risk of severe adverse events. Biocompatible vehicles offer an alternative approach for sustained drug delivery to target organs [24]. However, securely anchoring these vehicles to the target site remains an unresolved issue. Existing methods, such as adhering vehicles with surgical glue or suturing them onto the organ, may cause side effects like inflammation and fail to ensure long-term adhesion due to body movement and material degradation. A potential solution to these challenges lies in biocompatible wet-adhesive drug delivery platforms. These platforms can firmly adhere to the target organ, provide sustained drug release over an extended period, and degrade safely after the drug has been fully delivered.

In this study, we developed a dopamine-modified ECM designed for wet tissue adhesion and drug delivery. ECM-dopamine exhibited excellent biocompatibility both *in vitro* and *in vivo*, along with strong adhesion to various substrates. ECM-dopamine can serve as an effective platform for the delivery of macromolecules. Additionally, incorporating solid lipid nanoparticles (SLNs) loaded with drugs into ECM-dopamine enabled the sustained release of small molecules. *In vivo* imaging demonstrated prolonged release of the therapeutic agents from ECM-dopamine-SLN at the target site. When loaded with silvadene, an antimicrobial agent, ECM-dopamine significantly reduced inflammation and enhanced wound healing in a mouse skin excision model. Furthermore, implanting ECM-dopamine loaded with Insulin-like growth factor-1 into injured muscle tissue promoted skeletal muscle repair in a mouse volumetric muscle loss model. This study highlights ECM-dopamine as a bioactive and biocompatible material, suitable not only for drug delivery but also for a range of applications requiring wet adhesion.

2. Methods

2.1. ECM preparation

ECM was isolated from porcine hearts following an established protocol [17]. In brief, porcine ventricles were decellularized in Sodium dodecyl sulfate (Aladdin, China) and Triton X-100 (Aladdin, China) solutions. After complete cell removal, ECM was washed with deionized water and then lyophilized. ECM was pulverized in liquid nitrogen and digested by pepsin to generate a homogeneous ECM solution. The ultimate ECM concentration was 10 mg/ml. The ECM solution was neutralized and stored at −20 °C before use.

2.2. Dopamine modification

Dopamine hydrochloride (Aladdin, China) was dissolved in pH 6.0 1xPBS at room temperature. The final dopamine HCl concentration was 18.9 mg/ml 1-Ethyl-3-(3-dimethylaminopropyl)carbodiimide (EDC) (Aladdin, China) and N-Hydroxysuccinimide (NHS) (Aladdin, China) were dissolved in water to prepare stock solutions. Stock solutions were added to the dopamine solution at 1:100 dilution. In adhesion tests, the final EDC and NHS concentrations were 100 μM, 1000 μM, and 10,000 μM. Distinct crosslinker concentrations were studied to explore the optimal dosage. In the rest of the study, 100 μM EDC/NHS was used. ECM solution was added to the reaction system at 1:10 dilution. Samples in 50 ml conical tubes were reacted on a tube rotator for 6 h at room temperature. The rotation speed was set to 10 rounds per minute. After 6 h, samples were transferred to dialysis bags and dialyzed against distilled water for 2 days. The pH of distilled water was adjusted to 6.0 using 2 N HCl to suppress dopamine oxidation. The water was replaced 3 times. The cutoff molecular weight of the dialysis bag was 3.4 kDa. After dialysis, samples were lyophilized for 3 days and stored at 4 °C. Unmodified ECM samples were not treated by dopamine and EDC/NHS. They were diluted using pH 6.0 1xPBS, dialyzed against acidified water for 2 days, and lyophilized for 3 days.

2.3. Scanning electron microscopy

Lyophilized SLN, ECM, ECM-dopamine, or ECM-dopamine-SLN were adhered to the sample holder using carbon tape. After gold sputtering using a Leica EM SC050 (Leica, US.), samples were transferred to a Hitachi S3400 SEM (Hitachi, Japan). Samples were then imaged at 15.0 kV.

2.4. Fourier-transform infrared spectroscopy

Lyophilized samples were processed into KBr pellets before FTIR measurements. A PerkinElmer Spectrum 100 (PerkinElmer, US) was used for the measurements. Transmittance curves were recorded after calibration against air. The resolution was set to 2 cm^{-1}. Baseline corrections were performed using Spectragryph v1.2.15 (Spectroscopy Ninja, Germany).

2.5. X-ray diffraction spectroscopy

Samples were lyophilized and pulverized before XRD measurements. A Bruker D8 Advance X-ray Diffractometer with copper Kα radiation was used for the measurement. The signal was recorded from 10° to 80°2θ with a step size of 0.01°2θ and a time interval of 0.1 s. Voltage was set to 40 kV and current was set to 40 mA.

2.6. Adhesion test

Dry ECM-dopamine was placed on a clean glass slide and wetted with 100 μl of distilled water. A second clean glass slide was placed on top of ECM-dopamine. The assembly was then mounted onto an adhesive force

analyzer (HYTECH-03, Shanghai QingyiYuan Tech. Co., Ltd., China). The Slides were held in place by jaws or magnetic sample holders. Distilled water was added to the chamber to submerge the slides. After waiting for 3 min, pull or shear forces were measured. An n-butyl cyanoacrylate adhesive (3M, China) was employed to compared the ECM-dopamine with commercial tissue adhesives. For the pull strength test, the jaw's moving speed was set to 0.5 mm/min with a displacement of 3 mm. For the shear strength test, the speed was set to 3 mm/min and the displacement was 15 mm. Slides were cleaned between measurements. Three milligrams of dry ECM-dopamine were used for each run. ECM-dopamine between slides was imaged to measure the area.

In tissue adhesion tests, 3 mg of dry ECM-dopamine was attached to a pre-wetted finger. The finger was then pressed onto pig muscle, fat, or skin tissue. The tissue sizes were approximately 1 cm × 1 cm x 0.5 cm. Finger and porcine tissue were then submerged in water to test the wet adhesion.

2.7. Atomic force microscopy

Lyophilized ECM or ECM-dopamine were adhered to glass coverslips and loaded onto Bruker Dimension XR (Bruker, US). A spherical tip (Bruker MLCT-o10) was used. The tip diameter was 6 μm, sensitivity was 40 nm/V. The measurement depth was 10 nm. The extension and retraction curves were recorded.

2.8. Hemocompatibility test

Fresh sheep blood supplemented with citric acid was used to analyze the hemocompatibility. To analyze the hemolytic effects, 3 mg of ECM or ECM dopamine was incubated with 1 ml of diluted blood (1:10 dilution in 1xPBS) at 4 °C. Incubation was ended by hour 1, day 1, day 3, day 7, day 14, day 21, and day 28. Samples were centrifuged at 500 g for 5 min and the supernatants were collected. The light absorbance at 540 nm were measured using a microplate reader. PBS buffer was used as the negative control, and 100 μl of 0.2 % triton x-100 solution was used as the positive control.

The hemostatic effects were investigated using the blood sample containing 25 mM $CaCl_2$. One hundred microliters of the blood were added to ECM samples or PBS. The samples were incubated for 10 min at 37 °C. Afterward, 1 ml of 1xPBS was added to the samples and incubated for 10 min at 37 °C. The supernatant was then aspirated and the light absorbance was measured at 540 nm using a microplate reader.

2.9. Drug release kinetics

To investigate the exogenous protein release from ECM-dopamine, 1 mg of bovine serum albumin (BSA) dissolved in 25 μl of DI water was added to 3 mg of dry ECM-dopamine. The resulting mixture was lyophilized for 2 days. ECM (3 mg) containing BSA (1 mg) was employed as positive control, and ECM-dopamine (3 mg) without BSA was used as negative control. Samples were immersed in 0.5 ml of 1xPBS at room temperature. To study the protein release within 24 h, 100 μl of the buffer were sampled at 5 min, 15 min, 30 min, 1 h, 2 h, 4 h, 8 h, and 24 h. Fresh 1xPBS was added after each sampling. To investigate the long-term release, Samples were immersed in 1 ml of 1xPBS at room temperature. One milliliter of buffer was sampled at day 3, 5, 7, and 9. Fresh 1xPBS was added after sampling. The protein concentrations were measured using BCA assay. To estimated the release rate of IGF-1 from ECM and ECM-dopamine, 100 μg of dextran-FITC (4 kDa) (Proteintech, China) was embedded into 3 mg of ECM and ECM-dopamine. The sampling procedures are same as above, except the long-term release experiment was prolonged to 13 days.

Solid lipid nanoparticles (SLNs) were prepared following an established protocol [21]. In brief, cetyl palmitate (Inno-chem, China) and tocopheryl acetate (Inno-chem, China) were melted on a 60 °C hot plate with constant stirring. Eight milligrams of fluorescein (FITC) was added to 230 of mg cetyl palmitate and 120 μl tocopheryl acetate. After complete mixing, 6 ml of pre-heated 10 % Tween-20 (Inno-chem, China) solution was added dropwise to the lipids. Samples were stirred at 1000 rpm for 3 min and then sonicated for 2 min. Samples were subsequently cooled on ice, centrifuged, and resuspended in 8 ml 1xPBS. 30 μl of SLN-FITC were added to 300 μl of ECM-dopamine solution before lyophilization. After lyophilization, ECM-dopamine-SLN-FITC were submerged in 500 μl of 1xPBS. To investigate the short-term release, 50 μl of buffer was sampled at 5min, 10min, 30min, 60min, 120min, 240min, 480min, and 1440min. 50 μl of 1xPBS were added after each sampling. To investigate the long-term release, samples were incubated in 500 μl of 1xPBS and sampled on days 2, 4, 6, 8, 10, 12, and 14. The PBS buffer was completely replaced during the long-term experiment. All sampled buffers were kept in a fridge. The fluorescent signal was measured using a Tecan Spark Multimode Microplate Reader (Tecan, Switzerland). FITC standards were used to calculate the absolute FITC concentrations.

To modulate the drug release rate, lyophilized ECM-dopamine-SLN-FITC samples were incubated with crosslinking agents. Lyophilized ECM-dopamine-SLN-FITC (30 μl FITC + 300 μl ECM-dopamine) samples were treated with 1 ml of genipin (Aladdin, China) solution overnight at room temperature. Genipin solution was prepared by diluting a 50 mg/ml genipin-in-DMSO stock solution to concentrations of 5 mg/ml, 0.5 mg/ml, and 0.05 mg/ml using 1xPBS. Genipin solution was completely removed after crosslinking, and 1 ml of fresh 1xPBS was added to each sample. One hundred microliters of the buffer were sampled at 5min, 10min, 30min, 60min, 120min, 240min, 480min, and 1440min. The same volume of fresh 1xPBS was added after each sampling. All sampled buffers were measured immediately after the 1440min sampling.

2.10. ECM-dopamine-SLN-silvadene fabrication

Silvadene (Aladdin, China) was incorporated into SLNs using the same method as for FITC incorporation. Eight milligrams of Silvadene was added to 230 mg of cetyl palmitate and 120 μl of tocopheryl acetate. The resulting SLN-silvadene were suspended in 8 ml of DI water. The final Silvadene concentration was 1 mg ml^{-1} 300 μl of SLN-silvadene were added to 30 ml of ECM-dopamine solution and mixed by vortexing. The final Silvadene concentration in ECM-dopamine was approximately 0.01 mg Silvadene per 1 mg dry ECM, which is equivalent to the dosage found in commercialized Silvadene 1 % cream. Samples were lyophilized and stored at 4 °C until use. ECM-SLN-silvadene was prepared using the same method.

2.11. Ultraviolet–visible spectroscopy

Two milligrams of dry ECM, ECM-dopamine-SLN-silvadene, SLN-silvadene, or Silvadene were suspended in 2 ml of DI water. The sample was transferred to a glass cuvette and the UV–Vis absorbance was measured using a BioTek Synergy LX Multimode Reader (Agilent, US). Absorbance from 200 to 500 nm was measured at a sampling frequency of 2 nm. The cuvette was washed with ethanol and DI water between measurements.

2.12. Anti-microorganism test

Ten milligrams of ECM or ECM-dopamine-SLN-silvadene were first processed into 10 mm pallets. E.coli or S.aureus were diluted to a concentration of 10^6 CFU/ml using 1xPBS. 100 μl of diluted bacterial suspension was evenly spread across each LB agar plate. ECM samples were placed at the center of the plates and lightly pressed to ensure full contact with the agar surface. Plates were incubated in a 37 °C incubator for 24 h and imaged afterward.

2.13. ECM-dopamine digestion

One milligram of ECM-dopamine was digested in 1 ml of collagenase type I (Aladdin, China) or pepsin (Sigma-Aldrich, US) buffer. Collagenase type I buffer was prepared by dissolving 0.1 mg of collagenase type I (125 U mg^{-1}) in 1 ml of 1xPBS containing 36 mM $CaCl_2$. Pepsin buffer was prepared by dissolving 0.1 mg of pepsin in pH 2.0 DI water. Samples were incubated at 37 °C to accelerate the digestion. Digestion buffer was sampled at 1h, 2h, 4h, and 8h. 100 μl of digestion buffer was sampled from each tube. After each sampling, the same volume of fresh digestion buffer was added. Protein concentrations were measured using a Bradford assay (Beyotime Tech., China).

2.14. Cell compatibility test

One milligram of ECM-dopamine was rehydrated in 1xPBS and then transferred to a 48-well tissue culture plate. Samples were air-dried in the plate and disinfected under UV light in a bio-safety hood for 2 h. L929 cells were suspended in DMEM (Servicebio, China) supplemented with 5 % Fetal Bovine Serum (Zhejiang Tianhang Biotech. Co. Ltd., China) and 100 U/ml Penicillin-Streptomycin (Servicebio, China) [cell culture media]. The cell density was adjusted to 100,000 cells per milliliter. A 200 μl aliquot of cell suspension was added to each well. After overnight plating, cells were cultured in fresh cell culture media for 48 h, and then fixed using 4 % paraformaldehyde. After fixation, cells were stored in 1xPBS in a fridge before immunostaining.

2.15. In vivo imaging

Nanoparticles containing Biotin-PEG-Cy5 (MW 3400 Da, Aladdin, China) were prepared following the protocol described above. The final concentration was approximately 1 mg of biotin-PEG-Cy5 in 40 mg of lipids per 1 ml of PBS buffer. 1 ml of this buffer was added to 10 ml of ECM-dopamine solution before lyophilization. After lyophilization, samples were stored at 4 °C and used within 1 week.

Before surgery, mice were anesthetized using 4 % isofluorane and maintained via 2 % isofluorane. After immobilizing the limbs using surgical tapes, the hair on the abdomen was removed using a hair removal cream. The skin was then disinfected using 70 % ethanol and povidone-iodine. Approximately 1 cm incisions were made on the skin and muscle to expose the liver. Four milligrams of ECM-dopamine-SLN containing biotin-PEG-Cy5 was applied to the liver surface. Incisions were then closed using 6-0 sutures. In the control group, 300 μl of SLNs containing biotin-PEG-Cy5 (in 1x PBS) were injected into the liver after it was exposed, with a total of 6 injections administered. Mice were returned to their nest after recovering from anesthesia. Biotin-PEG-Cy5 distribution on days 1, 3, and 7 was assessed using a PerkinElmer IVIS Spectrum System. Mice were euthanized after the day 7 imaging. Major organs were harvested and imaged using the IVIS system. Total flux was measured using the Living Image software v. 4.4 (PerkinElmer, US.).

2.16. Skin excision model

All animal procedures were reviewed and approved by the Institutional Animal Care and Use Committee at Shanghai Jiaotong University (SJTU). The procedures adhered to the guidelines outlined in the Guide for the Care and Use of Laboratory Animals, 8th edition (NIH, US) [25].

Mice were housed in individual cages in a Specific Pathogen-Free Animal Research Facility at SJTU. Skin excision procedures were adapted from published protocols [26,27]. In brief, 8-week CD-1 mice were anesthetized using 4 % isoflurane and maintained via 2 % isoflurane. Hair on the back was removed using hair-removal cream. After disinfection using 70 % ethanol and povidone-iodine, a 10 mm circle was marked on the skin. The skin was excised using surgical scissors, and the wound was splinted using a sterilized silicone ring (10 mm inner diameter). The silicone ring was secured with interrupted 5-0 nylon sutures. Mice were returned to the cage after surgery. Wounds were dressed with 10 mg of dry ECM, ECM-dopamine, or ECM-dopamine-SLN-silvadene 6 h after excision. No treatment was applied to control mice. Mice were anesthetized before ECM dressing. Wounds were left open for the remainder of the experiment. Mice were imaged on days 1, 2, 4, 8, 10, 12, and 14 post-excision. Silicone rings were removed on day 8. The same rings were temporarily placed on top of wounds for reference on days 10, 12, and 14.

One hundred 50 μL of blood were collected on day 8 via retro-orbital sinus sampling after isoflurane-induced anesthesia. Blood cells were analyzed the same day using a Sysmex XN-1000V hematology analyzer (Sysmex, Germany). All mice were euthanized on day 14 post-excision.

2.17. Volumetric muscle loss model

One microgram of Insulin-like growth factor-1 [IGF-1] (Proteintech, China) suspended in 10 μl of DI water was added to 5 mg of ECM-dopamine or ECM. Samples were lyophilized and stored at −20 °C before use.

Volumetric muscle loss was created following published protocol [28]. In brief, after anesthetizing CD-1 mice using isoflurane, an incision was made on the rear limb to expose the tibialis anterior muscle. An approximately 3 mm × 6 mm defect was created in the tibialis anterior muscle using a 3 mm biopsy punch. ECM samples were implanted into the defect area. The incision on the skin was then closed using 6-0 absorbable sutures. Grip strength of the rear limbs was measured using a grip strength meter (Shanghai Xin Luan MDT Infotech LTD., China) on day 3, 7 and 19 post surgery. Gait and foot pressure were measured using TreadScan (CleverSys Inc., US.) on day 7 post surgery. All mice were euthanized on day 21 for histological analysis and flow cytometry.

2.18. Histological staining

After fixation using 4 % PFA, skin samples were embedded in O.C.T. compound (Sakura Finetek, US) and sectioned into 10 μm slices using a Cryotome (Leica CM1950, Germany). Samples were washed in distilled water 3 times and stained using an HE staining kit (Sbjbio Life Sciences, China) or an MT staining kit (Solarbio Life Sciences, China). Samples were mounted using neutral balsam (Solarbio Life Sciences, China) and imaged within a week.

2.19. Fluorescent immunostaining

Tissue sections were washed in 1xTBS 3 times, permeabilized in 1xTBS containing 0.1 % Triton X-100 [washing buffer], and then incubated in 1xTBS containing 10 % normal goat serum [blocking buffer] for 1 h at room temperature. Samples were incubated in primary antibody staining buffer for 2 h and in secondary antibody staining buffer for 1 h at room temperature. Staining buffers were prepared by diluting antibody stock solutions using 1xTBS containing 1 % bovine serum albumin (Inno-chem, China). Samples were then incubated in 1xTBS containing 0.5 μg ml^{-1} DAPI (Sigma-Aldrich, US.) for 10 min. Afterward, samples were washed in 1xTBS 3 times and mounted using anti-fading mounting media (Solarbio Life Sciences, China). Mouse α-smooth muscle actin, rabbit CD31, and rabbit vimentin antibodies were purchased from Proteintech (China). Goat anti-mouse Alexa Fluor 488 and goat anti-rabbit Alexa Fluor 568 secondary antibodies were purchased from ThermoFisher Scientific (China).

Cells in tissue culture plates were washed in 1xPBS, permeabilized in 1xPBS containing 0.1 % Triton X-100 for 15 min, incubated in phalloidin staining buffer (Yeasen, China) for 2 h, and in DAPI staining buffer for 10 min at room temperature. Cells were washed in 1xPBS 3 times and imaged on the same day.

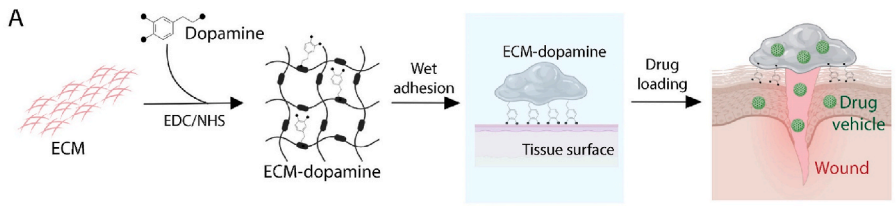

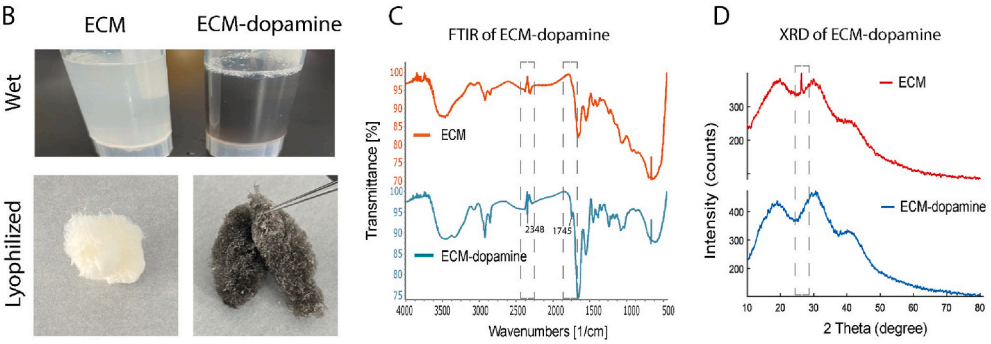

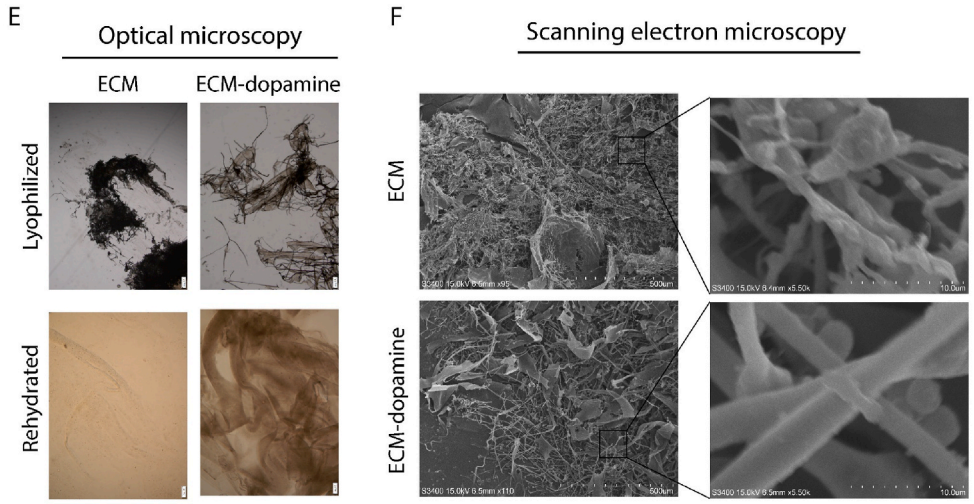

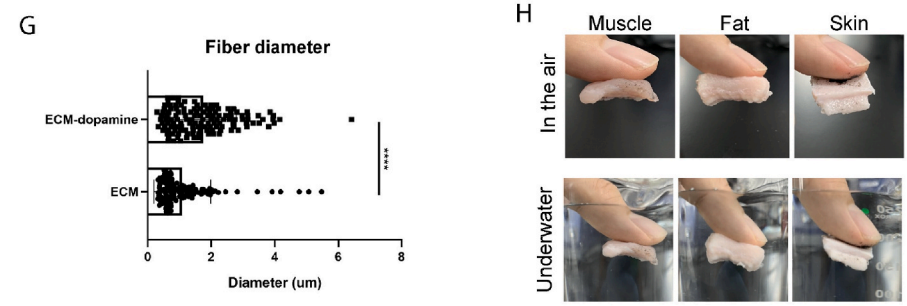

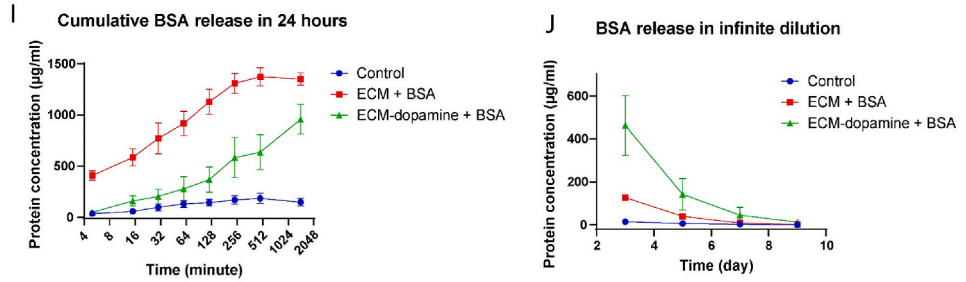

(caption on next page)

Fig. 1. ECM-dopamine fabrication and characterization. (A) Schematic representation of the experimental design. Dopamine molecules were conjugated to ECM via EDC/NHS chemistry. ECM-dopamine exhibited strong wet adhesion to tissue. Drugs incorporated into ECM-dopamine were capable of sustained release at the wound site. (B) The ECM solution turned from opaque white to dark brown following dopamine modification. ECM-dopamine formed an aerogel-like substrate after lyophilization. (C) FTIR spectroscopy revealed additional peaks around 2350 cm^{-1} and 1740 cm^{-1} in ECM-dopamine. (D) XRD analysis showed a sharp peak indicative of crystalline microstructure in ECM samples, while ECM-dopamine exhibited an amorphous microstructure. (E) Optical microscopy revealed entangled fibers in dry ECM-dopamine. Upon rehydration, ECM-dopamine remained intact, while ECM partially dissolved. (F) SEM showed a similar microstructure for both ECM and ECM-dopamine, with ECM-dopamine primarily consisting of fibers. (G) ECM-dopamine showed a broader distribution of fiber diameters compared to ECM. The average fiber diameter of ECM-dopamine was about 1.7 μm, which is significantly thicker than that of ECM. (H) Tissue-to-tissue adhesion in the air and underwater was also examined. Porcine muscle, fat, and skin were adhered to the finger using ECM-dopamine in both conditions. (I) The release rate of exogenous proteins from ECM-dopamine was assessed using BSA, with ECM-dopamine (without BSA) as the control. ECM-dopamine released proteins at a slower rate compared to ECM within 24 h. (J) Over a period from day 3 to day 9 in an infinite dilution experiment, ECM-dopamine released significantly more proteins compared to ECM. ($n = 3$ in panel I and J. T-test applied for panel G. ****$p < 0.0001$. Data are presented as mean ± SD.). (For interpretation of the references to color in this figure legend, the reader is referred to the Web version of this article.)

2.20. Flow cytometry

Freshly harvested muscles were minced in ice-cold 1xPBS using surgical scissors. Samples were digested with 1 mg/ml collagenase type II [>250U/mg] (Yeasen, China) and 1 mg/ml dispase for 1 h at 37 °C. After digestion, samples were filtered sequentially through 100 μm and 40 μm cell strainers (Falcon, US.). The digestion was neutralized with PBS containing 2 % BSA and 2 mM EDTA. Cells were washed once in 1xPBS containing 1 % BSA [staining buffer] and resuspended in 1xPBS buffer containing 1 % PFA and 2 % BSA for fixation. After fixation on ice for 10 min, cells were washed in staining buffer once and used within 24 h.

Before staining, cells were blocked in staining buffer containing Fc blocker (Proteintech, China) for 10 min on ice. Cells were then incubated with fluorophore-conjugated antibodies for 60 min on ice, washed in 1xPBS twice, and resuspended in 1 ml of 1xPBS. Flow cytometry analysis was performed using a BD LSRFortesse (US.) within 1 h after staining. PE anti-mouse CD45 antibody, CoraLite Plus 405 anti-mouse CD45 antibody, Per-Cyanine5.5 anti-mouse CD11b antibody, CoraLite Plus 647 anti-mouse Ly6G antibody, FITC anti-mouse MHC II antibody, CoraLite Plus 750 anti-mouse CD206 antibody were purchased from Protechtech (China). The flow cytometry data was analyzed using FlowJo v10.9.0 (BD, US.).

2.21. Optical microscopy

Chemically stained sections were imaged using an Olympus VS200 research slide scanner (Olympus, China) at 20X magnification. Whole sections were imaged. ECM samples and immunostained sections were imaged using a BX63 microscope (Olympus, China). Vessels were imaged at 20X magnification and fibroblasts were imaged at 40X magnification. High-resolution images were captured using an IXplore SpinSR confocal microscope (Olympus, China). Cells in culture plates were imaged using a Nikon Eclipse Ti2-E inverted fluorescence motorized microscope (Nikon, China) at 10X magnification. Images were analyzed using ImageJ v1.54f (National Institutes of Health, US).

2.22. mRNA sequencing

Mice skin samples were harvested on day 14 post-excision, flash-frozen in liquid nitrogen, and stored at −80 °C until use. RNA was extracted from 10 mg of tissue using TRIzol reagent (ThermoFisher, China). Sequencing was performed via Illumina Novaseq 6000 after assessing sample quality using NanoDrop 2000 (ThermoFisher, US) and Agilent 2100 Bioanalyzer (Agilent, US). Raw data were processed by fastp, HISAT2, and DESeq2 [29–31]. The threshold was set to q-value <0.05 and foldchange >2 or <0.5 to identify differentially expressed genes. GO, KEGG, Reactome, and WikiPathways analyses were performed using corresponding databases [32–35]. Gene Set Enrichment Analysis was performed using GSEA software [36].

2.23. Static analysis

Statistical analysis was performed using GraphPad Prism 8. Comparisons between two groups were made using *t*-test, and those between three or more groups were conducted using one-way ANOVA and Tukey's test. Two-way ANOVA and Tukey's test were used to compare total flux, ECM area, and wound size at different time points. All data are presented as mean ± standard deviation. Group sizes and p-values were shown in figure legends. Sample size was determined according to published works.

3. Results

3.1. ECM-dopamine fabrication and characterization

The wet-adhesive ECM-dopamine was synthesized via EDC/NHS-mediated crosslinking of ECM scaffold with dopamine molecules (Fig. 1A). The resulting ECM-dopamine adheres to wet tissue surfaces through dopamine-mediated bridging. The initial white-opaque ECM solution turned dark brown after EDC/NHS-mediated dopamine conjugation (Fig. 1B). The color change was probably due to dopamine conjugation and polymerization, which has been reported in previous studies [37]. The ECM-dopamine was subsequently processed into an aerogel-like substrate through dialysis and lyophilization. Dehydrating ECM-dopamine not only helps prevent the rapid oxidation of dopamine in aqueous environments but also enables it to be molded into various shapes [38]. Fourier Transform Infrared Spectrometry (FTIR) demonstrated an altered spectrum following dopamine conjugation. Peaks at 2330 cm^{-1} and 1740 cm^{-1} in the ECM-dopamine samples indicated the presence of C=O and C-N groups, which signify the formation of amide bonds through the EDC/NHS conjugation process (Fig. 1C). The microstructure of ECM-dopamine was examined using X-ray diffraction (XRD). A sharp peak that represents crystalline microstructure was observed in ECM samples but not in ECM-dopamine (Fig. 1D). This discrepancy may be attributed to the crystalline proteins present in the ECM samples [39]. Broad peaks in the range of 15–45° characterize the amorphous microstructure of fibrous proteins [40]. These results demonstrate successful dopamine conjugation and complete removal of unlinked dopamine salt.

Optical microscopy revealed that dry ECM-dopamine primarily consisted of fibers, whereas dry ECM samples displayed large chunks (Fig. 1E). Notably, ECM chunks were barely visible after rehydration, which probably suggests a relatively high solubility of unmodified ECM in aqueous environments. In contrast, ECM-dopamine was insoluble in water. Scanning Electron Microscopy (SEM) revealed that ECM-dopamine primarily consisted of large fibers (Fig. 1F). The fiber diameter in ECM-dopamine was approximately 1.7 μm, which is significantly thicker than ECM (Fig. 1G). In addition, both ECM and ECM-dopamine exhibited a similar porous microstructure under SEM, which suggests that ECM-dopamine, like ECM hydrogel, can be used to embed cells and drug vehicles [21]. Furthermore, tissue-to-tissue adhesion was examined. Porcine muscle, fat, and epidermis were adhered to fingers in the

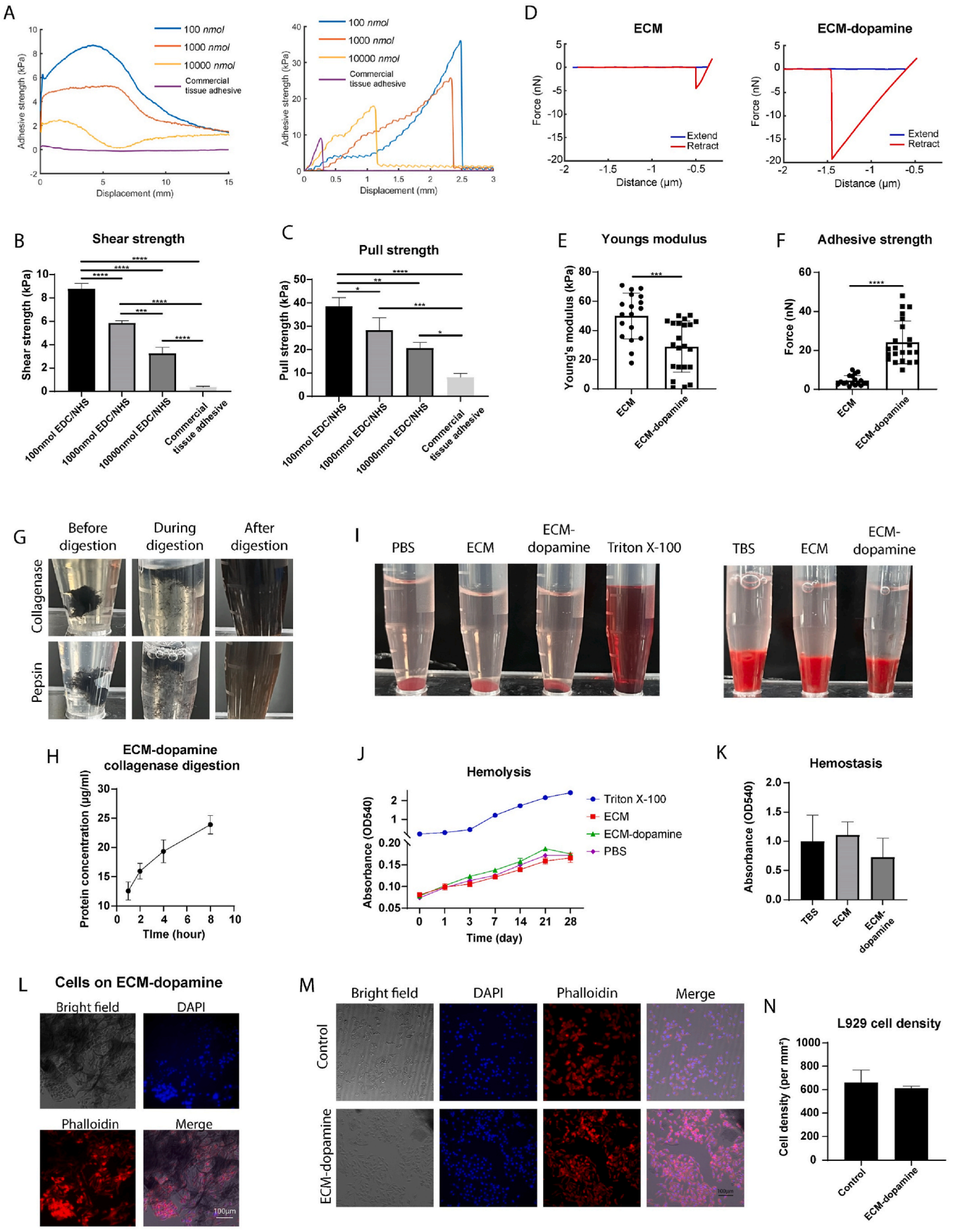

(caption on next page)

Fig. 2. ECM-dopamine revealed strong wet adhesion and good cell compatibility. (A) The adhesive force of ECM-dopamine was examined underwater. Dopamine molecules were conjugated to ECM via different amounts of EDC/NHS. (B) The shear strength was first measured. Increasing the concentration of EDC/NHS resulted in reduced adhesive strength. (C) Next, the pull strength was measured. A negative correlation was observed between the amount of EDC/NHS used and the adhesive strength. (D) Young's modulus was measured using atomic force microscopy. (E) ECM-dopamine exhibited a lower Young's modulus compared to ECM. (F) Dopamine modification increased the adhesive force by approximately 8 times. (G) Lyophilized ECM-dopamine can be degraded by collagenase or pepsin within 24 h under physiological conditions. (H) Protein release during collagenase-induced ECM-dopamine degradation was examined. A relatively consistent protein release was observed over 8 h. (I) The hemocompatibility of ECM-dopamine was examined using fresh sheep blood. ECM-dopamine exhibited similar (J) hemolytic and (K) hemostatic effects on the blood compared to the negative controls. (L) Next, cell compatibility was assessed using L929 cells. Large clusters of L929 cells were observed growing on ECM-dopamine. (M) Cells were cultured in the presence of ECM-dopamine for 2 days and imaged via fluorescent microscopy. (N) No significant difference in cell density was observed between the control and the ECM-dopamine group. ($n = 3$, One-way ANOVA and Tukey's test applied for panel B, C, and K, *t*-test applied for panel E, F, and N. *$p < 0.05$, **$p < 0.01$, ***$p < 0.001$, ****$p < 0.0001$. Data are presented as mean ± SD.)

air and underwater using ECM-dopamine (Fig. 1H). Collectively, these results indicate that ECM-dopamine maintained a microstructure similar to the original ECM scaffold, and can adhere to various tissues in the wet environment.

The feasibility of biomolecule delivery using ECM-dopamine was investigated using a protein release assay. ECM-dopamine containing bovine serum albumin (BSA) released fewer proteins compared to the ECM-BSA group within the first 24 h (Fig. 1I). In addition, only the ECM-dopamine-BSA group exhibited sustained protein release over the 24-h period. In the long-term protein release assay, ECM-dopamine released significantly more proteins compared to ECM and the no-BSA control groups (Fig. 1J). These results demonstrate that ECM-dopamine is capable of sustaining biomolecule release for at least 7 days.

3.2. ECM-dopamine exhibited strong wet-adhesion and high biocompatibility

The adhesive strength of ECM-dopamine in an aqueous environment was examined. Two glass slides were bonded using rehydrated ECM-dopamine, and the adhesive strength was measured underwater (Fig. 2A). To investigate the effect of crosslinker concentration on ECM-dopamine-mediated adhesion, dopamine and ECM were conjugated with varying concentrations of EDC/NHS. The corresponding crosslinker-to-dopamine molar ratios were 1:1 (100 nmol), 1:10 (1000 nmol), and 1:100 (10000 nmol). The shear strength of lyophilized ECM-dopamine was assessed first. EDC/NHS concentration was negatively correlated to shear strength (Fig. 2B). ECM-dopamine produced with 100 nmol EDC/NHS exhibited the highest shear strength of 8.5 kPa. The pull strength was also tested (Fig. 2C), and similarly, ECM-dopamine treated with 100 nmol EDC/NHS displayed the highest pull strength. These results indicate that ECM-dopamine serves as an effective wet adhesive, with its adhesive strength tunable through adjustments to crosslinker concentration.

The Young's modulus and adhesive force of ECM-dopamine treated with 100 nmol EDC/NHS were evaluated using atomic force microscopy (Fig. 2D). Dopamine modification slightly decreased the Young's modulus of ECM (Fig. 2E) while significantly enhancing its adhesive force (Fig. 2F). These findings suggest that ECM adhesion is facilitated by dopamine-mediated interactions, likely through hydrogen bonding with the substrate surface.

The biocompatibility of ECM-dopamine was evaluated *in vitro*, starting with its degradation profile. Dry ECM-dopamine samples were digested by collagenase type I or pepsin under optimal digestion conditions for 24 h (Fig. 2G). The insoluble ECM-dopamine transformed into a homogenous solution after digestion. The protein release rate during collagenase digestion was monitored (Fig. 2H). Collagenase treatment led to sustained protein release from ECM-dopamine over 8 h. These results suggest that ECM-dopamine is degradable under physiological conditions. Hemocompatibility was also assessed (Fig. 2I). Both ECM and ECM-dopamine exhibited minimal hemolysis compared to the negative control over 28 days (Fig. 2J). Similarly, ECM-dopamine did not affect hemostasis (Fig. 2K). These results demonstrate the high biosafety of ECM-dopamine for *in vivo* applications.

Next, cell viability was assessed. L929 mouse fibroblast cells were cultured with ECM-dopamine for 2 days. Cell clusters were observed on ECM-dopamine (Fig. 2L), suggesting that cells can adhere to ECM-dopamine. Cells cultured with ECM-dopamine exhibited similar cell density to control cells (Fig. 2M and N). These results indicate that ECM-dopamine has low cytotoxicity and, more importantly, cells can grow on or within ECM-dopamine, which is crucial for applications in cell delivery.

3.3. Solid lipid nanoparticle-incorporation enabled sustained release of small molecules from ECM-dopamine

ECM-dopamine alone is not suitable for the sustained release of small molecules due to its porous microstructure, which allows unbound molecules to diffuse rapidly and be released within hours through Fickian diffusion [41]. To enable the sustained release of small agents, solid lipid nanoparticles (SLNs) were employed as drug vehicles. The drug-loaded SLNs were prepared via an oil-in-water emulsion process followed by sonication (Fig. 3A). Peaks at 2920 cm^{-1}, 1735 cm^{-1}, and 940 cm^{-1} in the FTIR spectrum indicated the successful incorporation of cetyl palmitate-based SLNs into the ECM-dopamine-SLN samples (Fig. 3A). SLNs with an average size of approximately 300 nm were observed in ECM-dopamine-SLN samples using SEM (Fig. 3B).

Fluorescein (FITC) was used to assess drug release kinetics. FITC was released to the environment at a relatively steady rate for approximately 4 h before plateauing (Fig. 3C). In addition, FITC release persisted over 14 days in an infinite dilution experiment (Fig. 3D). To control the release rate, ECM-dopamine-SLN was treated with crosslinkers. Increasing the concentration of the crosslinking agent, genipin, resulted in reduced FITC release over 24 h (Fig. 3E). These results suggest that ECM-dopamine-SLN can serve as a platform for controlled delivery of small molecules.

The distribution and retention of drugs released by ECM-dopamine-SLN were investigated *in vivo*. SLNs containing biotin-PEG-Cy5 were utilized to minimize autofluorescence. Mice were imaged on days 1, 3, and 7 following the application of ECM-dopamine-SLN to the liver surface (Fig. 3F). SLNs containing biotin-PEG-Cy5 were injected into the liver as a control. The ECM-dopamine-SLN group showed significantly higher total flux than the SLNs group on days 3 and 7 after implantation (Fig. 3G). The total flux also remained more stable in the ECM-dopamine-SLN group over 7 days. Additionally, the distribution of biotin-PEG-Cy5 in major organs was investigated on day 7 post implantation. The liver exhibited significantly higher total flux compared to other major organs in both the ECM-dopamine-SLN and SLNs groups, with the highest total flux observed in the liver of the ECM-dopamine-SLN group (Fig. 3H). Collectively, the results indicate that adhering ECM-dopamine-SLN to the target organ enables sustained drug release for more than 7 days.

3.4. ECM-dopamine-SLN containing silvadene improved skin wound healing

As a proof of concept for potential applications, the delivery of small therapeutic agents was explored. Silvadene is an antimicrobial drug that is commonly used to prevent wound infections in patients with severe

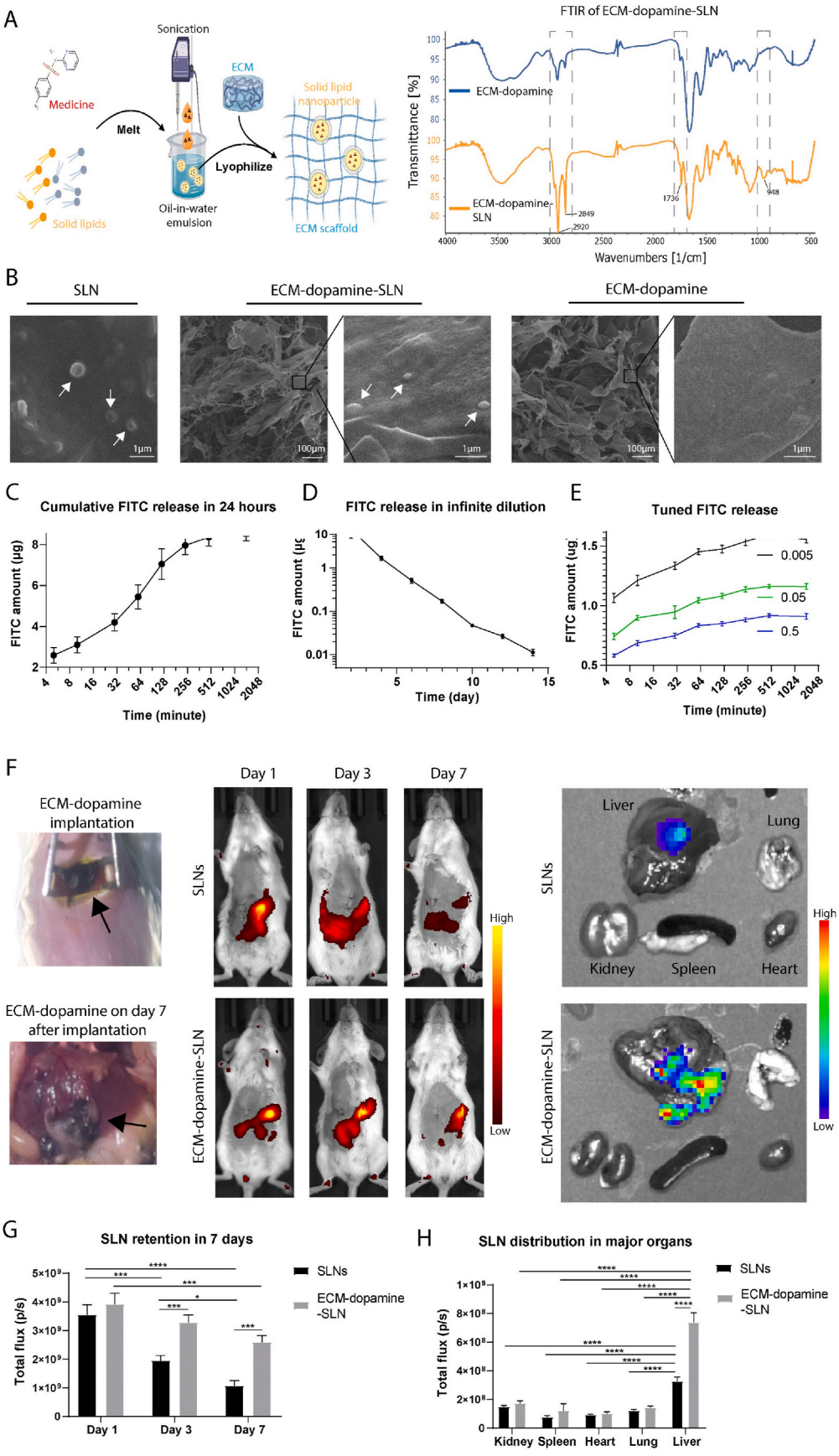

(caption on next page)

Fig. 3. ECM-dopamine-SLN facilitates sustained release of drugs into the target organ. (A) SLNs were prepared by oil-in-water emulsion and sonification of the drug-solid lipids mixture at 60 °C. FTIR spectroscopy indicated amplified peaks at 2920 cm^{-1}, 1735 cm^{-1}, and 940 cm^{-1} in ECM-dopamine-SLN samples. (B) The incorporation of SLNs did not alter the meshwork structure of ECM-dopamine; however, SLNs appeared as 300 nm white dots adhered to the ECM-dopamine. (C) SLNs containing fluorescein were utilized to assess the SLN release kinetics. ECM-dopamine-SLN slowly released FITC into the environment over 24 h. (D) A sustained release of FITC was observed over 14 days in an infinite dilution experiment. (E) The release rate of SLNs was modulated by genipin crosslinking. Lyophilized ECM-dopamine-SLN containing FITC was treated with 0.5 %, 0.05 %, or 0.005 % genipin buffer before measuring the FITC release kinetics. The FITC release rate was inversely correlated with genipin concentration. (F) SLN retention was investigated *in vivo*, with ECM-dopamine-SLN containing biotin-PEG-Cy5 adhered to the liver surface. The distribution of biotin-PEG-Cy5 in the body was examined via live imaging on days 1, 3, and 7 post implantation, along with an assessment of major organ distribution on day 7. (G) The ECM-dopamine-SLN group had higher total flux compared to the SLNs group on days 3 and day 7. In addition, the Cy5 signal faded slower in the ECM-dopamine-SLN group. (H) Biotin-PEG-Cy5 primarily accumulated in the liver in both SLNs and ECM-dopamine-SLN groups, with the liver in the ECM-dopamine-SLN group exhibiting the highest total flux. ($n = 3$, two-way ANOVA and Tukey's test applied, $^{*}p < 0.05$, $^{**}p < 0.01$, $^{***}p < 0.001$, $^{****}p < 0.0001$. Data are presented as mean ± SD.)

burns [42]. This agent is insoluble in water but can be loaded into SLNs. Silvadene was selected because of its well-established antimicrobial efficacy and safety profile [43,44]. UV–vis spectrometry demonstrated that SLN-silvadene was successfully incorporated into ECM-dopamine (Fig. S1A). The antimicrobial activity of ECM-dopamine-SLN-silvadene was tested against *S.aureus* and *E.coli* (Fig. S1B). ECM-dopamine-SLN-silvadene exhibited strong inhibition of *S.aureus* and *E.coli*. In contrast, ECM alone showed no anti-microbial effect. Together, the results demonstrate that ECM-dopamine can be processed into an anti-infective biomaterial by incorporating SLNs containing antimicrobial agents.

The therapeutic efficacy of ECM-dopamine-SLN-silvadene for wound healing was evaluated *in vivo*. Full-thickness wounds were created using a biopsy punch and surgical scissors [26]. Wounds were splinted with silicone rings to simulate human wound healing conditions. Six hours after excision, the wounds were dressed with dry ECM samples, with no additional protection applied. The *in vivo* experiment ended on day 14 (Fig. 4A). Wound healing was monitored by regular photographic documentation (Fig. 4B). Both ECM-dopamine and ECM-dopamine-SLN-silvadene treatments significantly reduced wound areas on day 8 post-excision compared to day 1 (Fig. 4C). Following the removal of silicone rings, the ECM-dopamine-SLN-silvadene group exhibited smaller wound sizes on days 10 and 12 than the other groups. Sample retention on the wounds was also assessed. Only a small fraction of unmodified ECM remained visible by day 2 post-excision (Fig. 4D). In contrast, areas of ECM-dopamine and ECM-dopamine-SLN-silvadene were not significantly changed from day 1 to day 4. As wound healing progressed, ECM-dopamine-SLN-silvadene became undetectable by day 12, which was earlier than in the ECM-dopamine group. Loading SLN-silvadene into ECM slightly accelerated the wound healing, but failed to increase the ECM retention (Figs. S1C–E). Overall, dopamine modification substantially improved ECM retention at the wound site, and the addition of antimicrobial agents in ECM-dopamine further accelerated open wound healing.

Skin wounds were examined histologically on day 14 post-excision. Hematoxylin and eosin (HE) staining was applied to visualize the epidermis and granulation tissue. Masson's trichrome (MT) staining was used to label collagen-rich areas (Fig. 4E). ECM-dopamine and ECM-dopamine-SLN-silvadene treatments promoted epidermal thickness (Fig. 4F) and granulation tissue formation (Fig. 4G) compared to the control. Furthermore, ECM-dopamine and ECM-dopamine-SLN-silvadene treatments significantly enhanced collagen deposition in comparison to both the control and ECM-only treatments (Fig. 4H). The presence of myofibroblasts and vasculatures was also assessed (Fig. 4I). ECM-dopamine and ECM-dopamine-SLN-silvadene groups showed lower myofibroblast-to-fibroblast ratios compared to the control and ECM-only groups (Fig. 4J), with the ECM-dopamine-SLN-silvadene group exhibiting the lowest ratio. In addition, both ECM-dopamine and ECM-dopamine-SLN-silvadene treatments increased vessel area compared to the control, whereas ECM-only treatment did not improve vascularization (Fig. 4K). These results indicate that ECM-dopamine and ECM-dopamine-containing antimicrobial agents accelerate the comprehensive repair of open wounds.

The transcriptomes of ECM-dopamine-SLN-silvadene and control groups were analyzed on day 14 post-excision, revealing **268 differentially expressed genes** (Figs. S2A and S2B). ECM-dopamine-SLN-silvadene significantly affected genes associated with the immune response and extracellular matrix remodeling (Fig. 4L). Gene Set Enrichment Analysis was conducted to identify biological processes that are influenced by ECM-dopamine-SLN-silvadene treatment (Fig. 4M). Control mice exhibited higher transcriptional activities in genes involved in fungal defense and collagen deposition. On the other hand, ECM-dopamine-SLN-silvadene group showed elevated transcription of genes related to epithelial cell differentiation. These results suggest that ECM-dopamine-SLN-silvadene helps mitigate microbial infection in wounds. Besides, the improved healing in ECM-dopamine-SLN-silvadene group was evidenced at the transcriptional level by reduced collagen formation and enhanced cell differentiation [45]. Additionally, Wikipathway enrichment analysis suggested that ECM-dopamine-SLN-silvadene modulated key pathways associated with differentiation and proliferation, including the mitogen-activated protein kinase (MAPK), epidermal growth factor receptor 1 (EGFR1), and G protein-coupled receptor (GPCR) pathways (Figs. S2C–E). In summary, ECM-dopamine-SLN-silvadene not only suppressed microbial infections but also accelerated wound healing. These therapeutic effects are probably mediated through GPCR, EGFR, and Mapk signaling pathways.

3.5. ECM-dopamine did not induce inflammation in vivo

Blood cell analysis was conducted on day 8 post-excision to assess inflammatory responses. Red blood cells and platelets were measured via hydrodynamically focused impedance measurements (Fig. 5A), and white blood cells were quantified using fluorescent flow cytometry (Fig. 5B). Neither ECM nor its derivatives influenced the count of white blood cells (Fig. 5C) or red blood cells (Fig. 5D). Both the ECM-only and ECM-dopamine-SLN-silvadene groups showed an increase in platelet count (Fig. 5E) and a reduction in the platelet-large cell ratio (Fig. 5F) compared to the control group. The observed increase in platelet numbers may indicate accelerated wound healing [46,47]. Larger platelets are typically more active than smaller ones [48]. Although the exact prognostic value remains undetermined, the increased platelet-large cell ratio is probably associated with various diseases, including coronary artery disease [49]. In this context, the altered platelet-large cell ratio may suggest delayed healing by day 8.

White blood cell subsets were examined. No significant differences were observed in neutrophil (Fig. 6G), lymphocyte (Fig. 6H), or eosinophil (Fig. 6I) counts across the groups. Nevertheless, ECM-dopamine-SLN-silvadene significantly increased monocyte count in comparison to control and ECM-only groups (Fig. 6J). While abnormal monocyte count is associated with infectious diseases and blood disorders, increased monocyte density in the wound area can benefit tissue healing by promoting angiogenesis and macrophage differentiation into reparative phenotypes [50,51]. Overall, these findings indicate that ECM-dopamine does not elicit an inflammatory response *in vivo*.

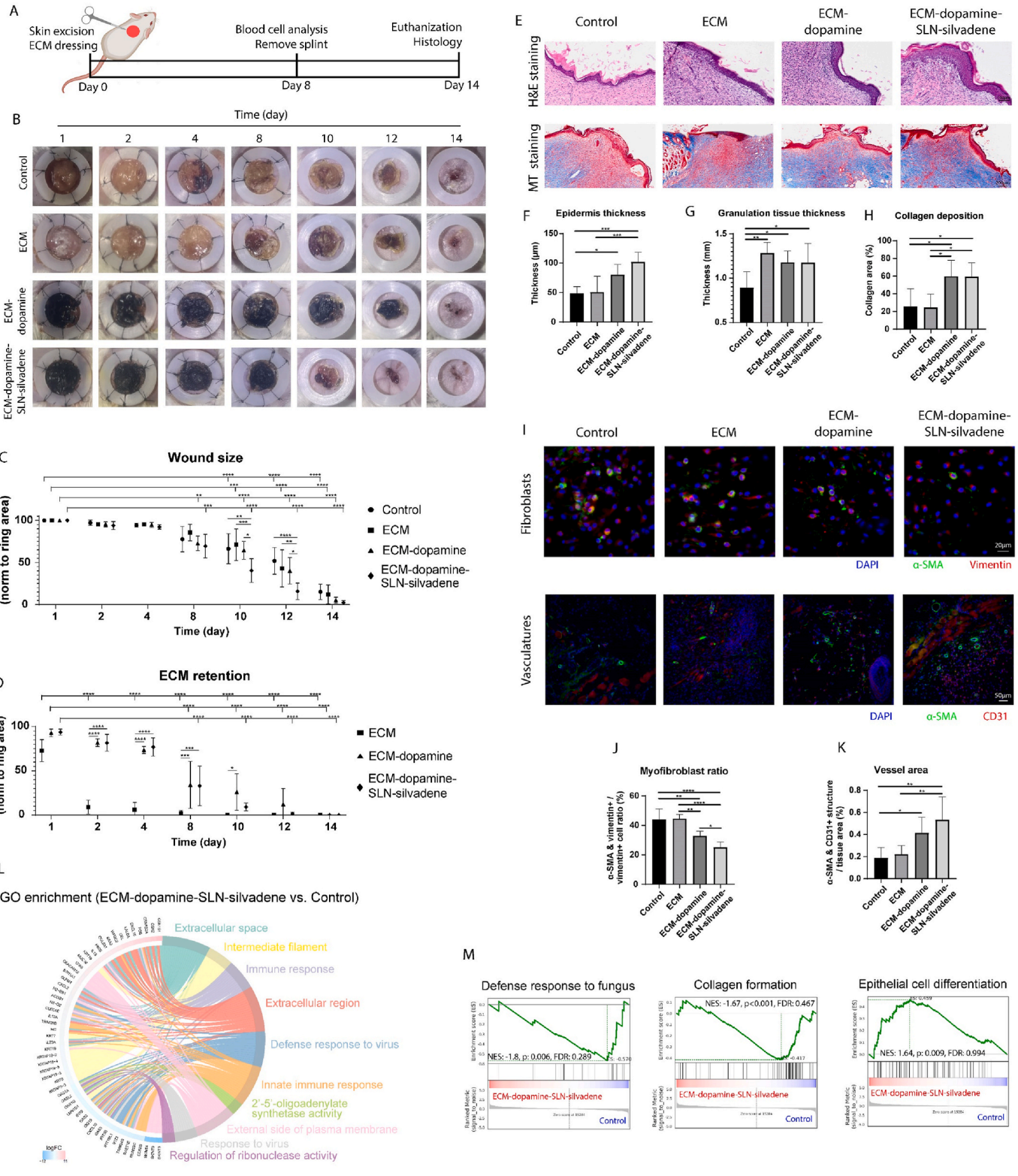

(caption on next page)

Fig. 4. ECM-dopamine-SLN loaded with antimicrobial promoted skin wound healing. (A) Experimental design. A 10 mm silicone ring was used to splint the wound after skin excision. ECM, ECM-dopamine, or ECM-dopamine-SLN-silvadene was applied 6 h after excision. Silicone rings were removed, and blood cell counts were analyzed on day 8. All mice were euthanized on day 14 for histological analysis. (B) Wound healing was regularly monitored through imaging. (C) Wound size over 14 days. ECM-dopamine and ECM-dopamine-SLN-silvadene treatments reduced wound sizes on day 8 compared to day 1. After silicone ring removal, the ECM-dopamine-SLN-silvadene group demonstrated significantly accelerated wound healing compared to other groups. (D) ECM retention was also examined. Non-modified ECM was largely absent by day 2 and barely detectable thereafter, while ECM-dopamine and ECM-dopamine-SLN-silvadene remained visible throughout the entire healing process. (E) Hematoxylin and eosin staining, as well as Masson's trichrome staining were performed to evaluate wound healing process. (F) ECM-dopamine increased epithelial thickness compared to the control, with further improvements observed in the ECM-dopamine-SLN-silvadene group. (G) ECM and its derivatives increased granulation tissue thickness in comparison to the control. (H) Collagen deposition, as indicated by MT staining, was notably higher in ECM-dopamine groups (with or without silvadene) compared to both the ECM-only and control groups. (I) Myofibroblasts and vasculatures were examined via immunostaining. (J) The ECM-dopamine-SLN-silvadene group exhibited the lowest myofibroblast to fibroblast ratio. Besides, ECM-dopamine lowered the myofibroblast ratio compared to the control and ECM-only treatments. (K) Both ECM-dopamine and ECM-dopamine-SLN-silvadene increased vessel area compared to the control, with ECM-dopamine-SLN-silvadene treatment showing a greater vessel area than ECM treatment. (L) mRNA sequencing revealed that ECM-dopamine-SLN-silvadene altered the transcription of genes related to extracellular matrix remodeling and inflammation, as shown by Gene Ontology analysis. (M) Gene Set Enrichment Analysis demonstrated that ECM-dopamine-SLN-silvadene suppressed the transcription of genes associated with fungus defense and collagen production. In contrast, ECM-dopamine-SLN-silvadene facilitated the transcription of genes related to epithelial cell differentiation. (n = 6 in panel C and D, two-way ANOVA and Tukey's test applied. n = 6 in panel F, G, H, J and K, one-way ANOVA and Tukey's test applied. *$p < 0.05$, **$p < 0.01$, ***$p < 0.001$, ****$p < 0.0001$. Data are presented as mean ± SD.)

3.6. ECM-dopamine containing insulin-like growth factor-1 promoted muscle repair after volumetric muscle loss

The potential application of ECM-dopamine in macromolecule delivery and tissue repair was explored using a skeletal muscle injury model, aimed at addressing the lack of effective treatment strategies for volumetric muscle loss. While ECM-dopamine provides a scaffold for cell support, it may not effectively guide cell proliferation and differentiation. To enhance myocyte growth, insulin-like growth factor-1 (IGF-1), a central regulator of muscle repair, was incorporated into ECM-dopamine [52,53]. As demonstrated by the dextran-FITC release experiment (Figs. S3A and B), ECM-dopamine was able to release loaded proteins over a period of at least 13 days, which is sufficient to support the early stages of muscle repair. Following ablation of the tibialis anterior muscle, lyophilized ECM samples were implanted into the defect (Fig. 6A). Rear limb function was measured using a grip strength meter (Fig. 6B and Fig. S3C). ECM-dopamine-IGF-1 treatment improved peak force in the rear limbs compared to the control on day 7 post-injury (Fig. 6C).

Notably, the ECM-dopamine-IGF-1 group exhibited a significantly increased force from day 3 to day 7, indicating accelerated healing of the rear right limb. Foot pressure was measured using a video-based gait analysis system (Fig. 6D). ECM-dopamine-IGF-1 treatment increased the pressure in the rear right foot compared to the control and ECM treatment on day 7 post surgery (Fig. 6E). ECM-dopamine also exhibited a trend of improving foot pressure compared to the control. These results demonstrate that ECM-dopamine-IGF-1 accelerates the functional recovery of skeletal muscles after volumetric muscle loss.

Myogenesis, fibrosis, and immune cells were examined to gain insights into the ECM-dopamine-IGF-1-mediated healing process. Muscular cells were stained with H&E staining and fibrotic tissue was labeled by MT staining (Fig. 6F). ECM, ECM-dopamine, and ECM-dopamine-IGF-1 treatments increased the diameter of myocytes in the defect area, with ECM-dopamine-IGF-1 treatment exhibiting the highest myocyte diameter (Fig. 6G). Additionally, only ECM-dopamine-IGF-1 significantly reduced the fibrotic area compared to the control (Fig. 6H). Given the crucial role of immune cells in muscle regeneration and scar formation, T cells and macrophages in the injury and border zones were analyzed using flow cytometry (Fig. 6I). $CD45^+$ cells were defined as immune cells (Fig. S3A). ECM-dopamine-IGF-1 group showed a higher number of CD45+$CD4^+$ T cells than the control and sham groups (Fig. 6J). However, the percentage of T cells among total immune cells was lower in ECM-dopamine-IGF-1 group (Fig. 6K). Next, CD45+CD4-Ly6G-CD11b + MHC II + macrophages were examined. ECM, ECM-dopamine, and ECM-dopamine-IGF-1 groups exhibited a trend toward increasing the percentage of macrophages compared to the control (Fig. S3B). Notably, ECM-dopamine-IGF-1 had the highest number of M2-like macrophage in all the groups (Fig. 6L). Although both ECM-dopamine and ECM-dopamine-IGF-1 groups had higher percentages of M2-like macrophages, the difference between ECM-dopamine and the control group was less pronounced than the difference in macrophage number (Fig. 6M). In summary, the results demonstrate that releasing IGF-1 via ECM-dopamine improves skeletal muscle repair by enhancing myocyte growth and inhibiting extensive scarring, likely through the modulation of M2-like macrophages.

4. Discussion

In this study, we developed an ECM-derived biomaterial that combines wet tissue adhesion with sustained drug delivery. Previous studies have shown that dopamine functionalization provides an effective approach for creating wet adhesive hydrogels [54,55], and that ECM-derived materials accelerate organ repair [56,57]. Nevertheless, to our best knowledge, an ECM-derived biocompatible wet adhesive designed for controlled drug delivery and tissue repair following traumatic tissue damage has not been reported. ECM-dopamine holds potential applications beyond wound healing, such as anchoring medical devices post-implantation. Additionally, drugs can be incorporated into ECM-dopamine to enable various therapeutic applications, including infection prevention and tissue regeneration.

Controlled and target-specific drug delivery remains a major challenge in advancing drug delivery systems [58]. ECM-dopamine can serve as a reservoir for drug-loaded nanocarriers, enabling target-specific drug delivery. As expected, small biomolecules delivered via ECM-dopamine-SLN predominantly accumulate in the target organ and remain there for an extended duration. Furthermore, the drug release rate can be tuned by adjusting the crosslinking density of the ECM-dopamine-SLN scaffold. This effect is likely due to the increased physical entanglement between fiber proteins, a phenomenon observed in drug release studies involving hydrogels and polymer systems [59,60]. A nature-derived crosslinking agent, genipin, was used in this study because of its relatively low cytotoxicity [61]. Future optimization of the crosslinking conditions may enable the production of ECM-dopamine-SLN that releases drugs over several months, making it better suited for treating chronic conditions such as heart failure. Beyond SLNs, other drug delivery vehicles can be incorporated into ECM-dopamine to achieve controlled release of a wider range of therapeutics. For instance, IGF-1 can be encapsulated within alginate microspheres to facilitate sustained release of the biomolecule.

ECM-derived biomaterials retain extracellular growth factors from their source tissue, enabling them to stimulate cell growth and direct differentiation in injured organs [16,62]. Consequently, ECM materials like ECM-dopamine offer more than just biocompatible adhesion; they also serve as platforms for modulating the healing process. Previous

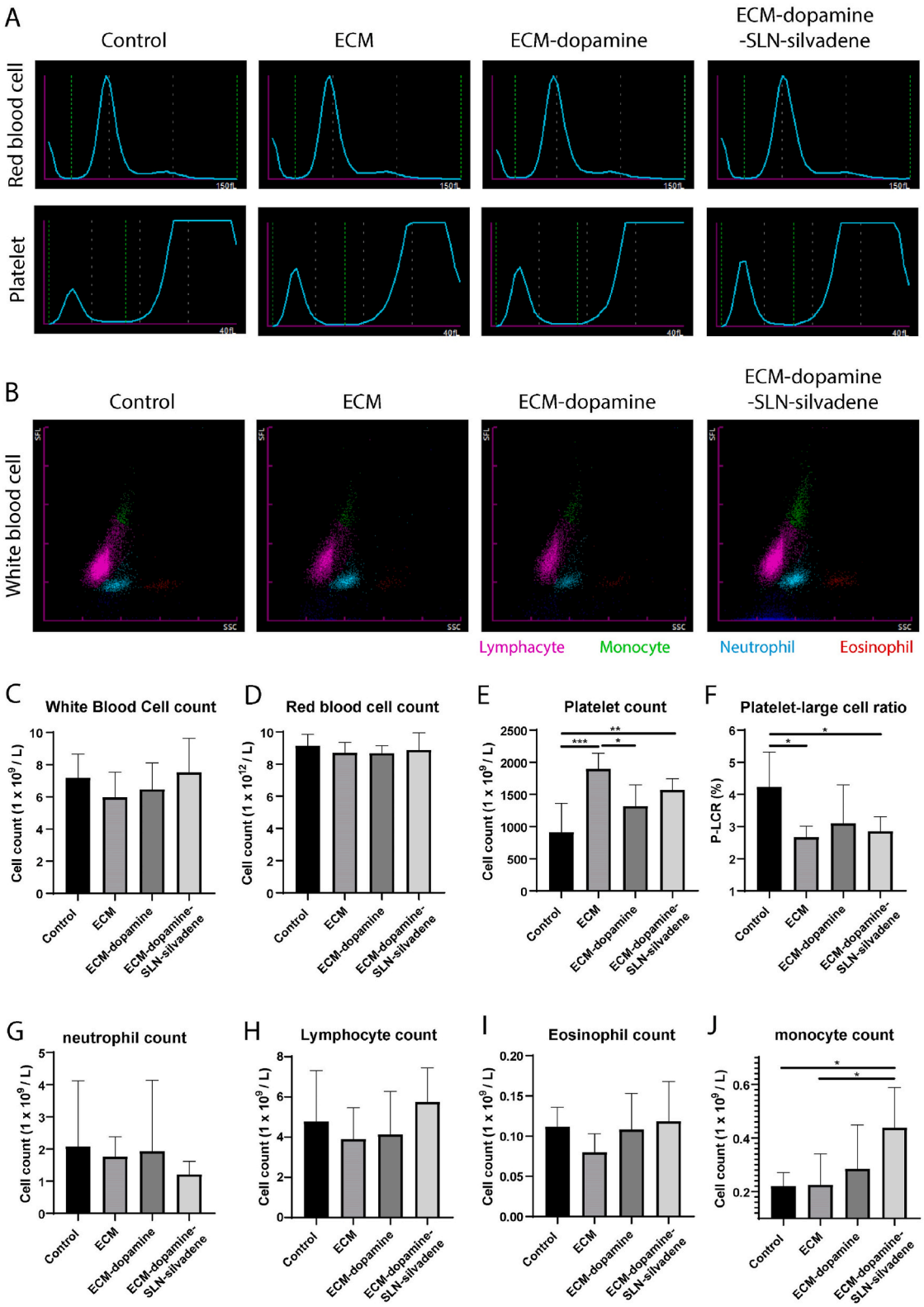

Fig. 5. Blood cell analysis on day 8 post-skin injury. (A) Red blood cells and platelets were analyzed via hydrodynamically focused impedance measurements. (B) White blood cells were analyzed using fluorescent flow cytometry. ECM treatments did not affect (C) white blood cell and (D) red blood cell counts. (E) Platelet counts were elevated in both ECM-dopamine-SLN-silvadene and ECM-only groups compared to the control. (F) The platelet-large cell ratio decreased in these same groups relative to the control. (G) Neutrophil, (H) lymphocyte, and (I) eosinophil counts did not differ significantly across the treatment groups. (J) However, ECM-dopamine-SLN-silvadene increased monocyte count compared to the control and ECM-only groups. (n = 6 in panel C, D, E, F, G, H, I and J, one-way ANOVA and Tukey's test applied, *$p < 0.05$, **$p < 0.01$, ***$p < 0.001$. Data are presented as mean ± SD.). (For interpretation of the references to color in this figure legend, the reader is referred to the Web version of this article.)

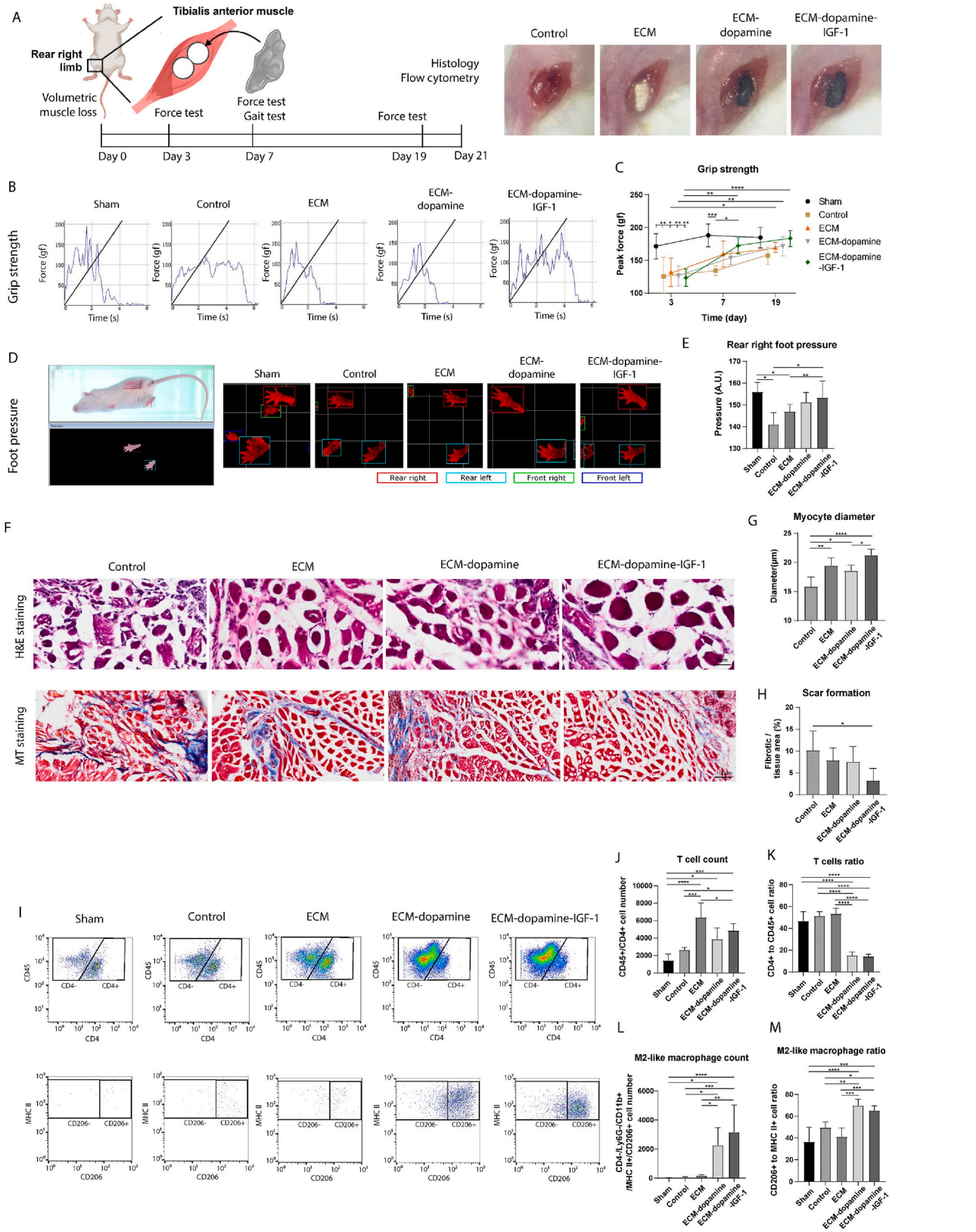

(caption on next page)

Fig. 6. ECM-dopamine loaded with insulin-like growth factor improved skeletal muscle repair. (A) Experimental design. Volumetric muscle loss was established by surgical ablation of tibialis anterior muscle using a 3 mm biopsy punch. ECM samples were implanted into the defect. (B) The grip strength of rear limbs was measured using a grip strength meter. (C) Volumetric muscle loss resulted in significantly reduced peak force on day 3. ECM-dopamine-IGF treatment promoted force recovery compared to the control on day 7 after surgery. (D) Mice gait was evaluated using a video-based gait analysis system. (E) ECM-dopamine and ECM-dopamine-IGF treatments significantly increased rear right foot pressure compared to the control on day 7. (F) Myocyte diameter and scar formation on day 21 post-surgery were examined using H&E staining and MT staining. (G) Both ECM and ECM-dopamine treatments increased myocyte diameter in the injury area compared to the control, with ECM-dopamine-IGF group exhibiting the highest myocyte diameter. (H) Fibrotic area was significantly reduced in the ECM-dopamine group compared to the control. (I) The population of various immune cells was analyzed using flow cytometry. (J) ECM and ECM-dopamine-IGF treatments promoted the T cell number compared to the control. (K) The percentage of T cells within $CD45^+$ immune cells was lower in ECM-dopamine and ECM-dopamine-IGF groups than in the other groups. (L) Both ECM-dopamine and ECM-dopamine-IGF treatments increased the number of M2-like macrophages compared to other treatments. (M) Only ECM-dopamine group exhibited a higher percentage of M2-like macrophages compared to the control. ($n = 5$ in panel E, G, H, J, K, L and M, one-way ANOVA and Tukey's test applied, $n = 5$ in panel C, two-way ANOVA and Tukey's test applied. *$p < 0.05$, **$p < 0.01$, ***$p < 0.001$, ****$p < 0.0001$. Data are presented as mean ± SD.)

studies have indicated that injecting ECM hydrogel derived from regenerative hearts promotes cardiac regeneration after myocardial infarction [17,63]. In this study, the ECM was sourced from adult porcine ventricles, which contain more ECM regulators and fewer ECM-affiliated proteins than the small intestine, a tissue more similar to skin [64]. We assume that using ECM derived from epithelial tissue may further improve skin wound healing. Similarly, utilizing ECM derived from skeletal muscle might further improve the therapeutic efficacy of ECM-dopamine for volumetric muscle loss. Nevertheless, *in vivo* studies are required to verify these hypotheses.

ECM-dopamine shows great potential as a wet tissue adhesive for clinical applications. The safety of ECM hydrogel has been studied in pre-clinical and clinical trials [19,65]. ECM has demonstrated low immunogenicity in porcine myocardial infarction models and human patients. In this study, ECM-dopamine dressing did not trigger an inflammatory response following skin excision. Nevertheless, further investigation is required to assess its long-term immunological effects before clinical application. Moreover, robust cell growth was observed on ECM-dopamine. This implies that ECM-dopamine provides binding sites and growth factors to cells. Because of its relatively high biocompatibility, ECM-dopamine can be used to adhere other substrates to organ surfaces, offering a less invasive alternative for drug delivery to vital organs. Current methods for delivering therapeutic agents into organs, such as intramyocardial injection, involve invasive procedures that pose risks of adverse events [66]. Delivering drugs using less invasive strategies, like adhesive ECM-dopamine patches, could lower the risk of adverse events. In addition, ECM-dopamine may serve as an alternative to traditional tissue glues. The adhesive strength of ECM-dopamine may be further enhanced by conjugating stronger wet-adhesive groups. Overall, ECM-dopamine offers a versatile platform that can be optimized for a wide range of therapeutic purposes.

The accelerated skin wound healing observed in this study was associated with suppressed microbial infection and enhanced extracellular matrix remodeling. Silvadene, an insoluble antibacterial agent, was used in the *in vivo* experiments, and its antimicrobial properties probably contributed to the improved wound healing by ameliorating inflammation caused by infections in open wounds. The difference between the control and experimental groups may become more significant in models of infected or diabetic wounds. However, this study primarily focused on wet adhesion and biocompatibility, leaving the therapeutic potential of ECM-dopamine-SLN-silvadene in other skin injury models unexplored. Despite this, ECM-dopamine, combined with antimicrobial agents, shows promise as a therapy for chronic skin injuries. Several genes associated with cell differentiation and proliferation were influenced by ECM-dopamine-SLN-silvadene. G protein-coupled receptors (GPCRs), which bind ligands such as hormones, lipids, and carbohydrates, are involved in a variety of skin pathologies, including injury, inflammation, and carcinoma [61,62]. Interestingly, GPCRs transactivate the epidermal growth factor receptor (EGFR), one of the key pathways modulated by ECM-dopamine-SLN-silvadene [63]. In addition, GPCRs play a critical role in regulating the mitogen-activated protein kinase (MAPK) pathway, which is essential for cell proliferation and differentiation [64]. The transcriptome data suggest that GPCRs have a significant role in skin wound healing, likely with MAPK and EGFR acting as downstream effectors. Because targeting GPCRs in the skin remains challenging, investigating their downstream pathways may reveal new targets for treating skin diseases. However, further validation using more specific methodologies is required to confirm their activation and interactions.

The treatment of volumetric muscle loss remains a significant challenge due to the lack of effective strategies for restoring lost muscle tissue [67]. ECM-dopamine not only provides a scaffold for proliferating myocytes and infiltrating immune cells but also serves as a delivery platform for exogenous therapeutic agents. Typically, IGF-1 and its delivery vehicles are administered via intramuscular injection to promote muscle repair [52,68]. However, maintaining IGF-1 levels in the muscle requires repeated injections, which can be inconvenient and painful. ECM-dopamine provides a potential solution for the sustained release of growth factors at the injury site. Our study demonstrates that ECM-dopamine loaded with IGF-1 significantly accelerates the healing of injured skeletal muscle. The observed increase in myocyte diameter and decrease in fibrosis in the ECM-dopamine-IGF-1 group likely result from the sustained release of IGF-1, which promotes skeletal muscle protein synthesis and activates satellite cells [69]. Additionally, this study also indicates that ECM-dopamine modulates immune cell accumulation in the muscle. Macrophages play a crucial role in muscle regeneration, but their exact function during the repair of volumetric muscle loss remains poorly understood. Our study suggests that the increased polarization of M2-like macrophages in the later stages of muscle repair is associated with promoted functional recovery of skeletal muscles. Similar increases in M2-like macrophage polarization have been observed in regenerating muscles following ischemic injury [70,71]. However, further investigation is needed to better understand the macrophage population at various time points after volumetric muscle loss and the specific role of the M2 macrophage subtype in muscle repair.

5. Conclusion

In this study, we developed a novel wet tissue adhesive, ECM-dopamine, with excellent biocompatibility and the capability to function as a drug delivery platform. *In vitro* and *in vivo* drug delivery assays demonstrated that ECM-dopamine enables sustained drug release for at least seven days at the target organ. Adhesion tests confirmed that ECM-dopamine adheres strongly to various tissue types, including skin, muscle, and fat. *In vivo* experiments further revealed that dopamine modification significantly enhanced ECM retention post-implantation. Incorporating antimicrobial agents into ECM-dopamine effectively suppressed infection and accelerated skin wound healing. Additionally, ECM-dopamine loaded with insulin-like growth factor-1 improved skeletal muscle repair following volumetric muscle loss, likely through the modulation of M2-like macrophage polarization. These findings highlight the potential of ECM-dopamine as a multifunctional biomaterial for regenerative medicine applications.

CRediT authorship contribution statement

Xinming Wang: Funding acquisition, Data curation, Conceptualization. **Haonan Zhang:** Methodology, Data curation. **Weichang Xie:** Methodology, Data curation. **Bei Qian:** Resources, Methodology. **Shixing Huang:** Resources, Methodology. **Qiang Zhao:** Investigation, Funding acquisition. **Xiaofeng Ye:** Supervision, Funding acquisition.

Funding

This work was Sponsored by the National Science Foundation for Distinguished Young Scholars of China (82125019); National Key Research and Development Program of China (2022YFA1105100); National Natural Science Foundation of China (82402485); Shanghai Pujiang Program (23PJ408200) from the Science and Technology Commission of Shanghai Municipality, China; Faculty Investment Fund (RC20220018) from Ruijin Hospital, School of Medicine, Shanghai Jiaotong University, China.

Declaration of competing interest

The authors declare that they have no known competing financial interests or personal relationships that could have appeared to influence the work reported in this paper.

Acknowledgment

We acknowledge the support of Feiyang Xue and other staff at the Instruments Center in the School of Life Sciences and Biotechnology at Shanghai Jiaotong University, China for SEM and microscopy. We thank the staff at Laboratory Animal Center at Shanghai Jiaotong University, China for the histological analysis. We thank OE Biotech, China for assisting with transcriptome analysis.

Appendix A. Supplementary data

Supplementary data to this article can be found online at https://doi.org/10.1016/j.mtbio.2025.101734.

Data availability

Data will be made available on request.

References

[1] C. Prevaldi, C. Paolillo, C. Locatelli, G. Ricci, F. Catena, L. Ansaloni, G. Cervellin, Management of traumatic wounds in the emergency department: position paper from the academy of emergency medicine and Care (AcEMC) and the world society of emergency surgery (WSES), World J. Emerg. Surg. 11 (1) (Jun. 2016) 1–6, https://doi.org/10.1186/S13017-016-0084-3/TABLES/4.

[2] A. Nair, A. Dahiya, P. Yadav, N. Sharma, B.S. Butola, Materials for the management of traumatic Wounds: a descriptive review, Eur. Polym. J. 222 (Jan. 2025) 112475, https://doi.org/10.1016/J.EURPOLYMJ.2023.112475.

[3] A. Moriscot, E.H. Miyabara, B. Langeani, A. Belli, S. Egginton, T.S. Bowen, Firearms-related skeletal muscle trauma: pathophysiology and novel approaches for regeneration, npj Regenerative Medicine 2021 6 (1) (Mar. 2021) 1–17, https://doi.org/10.1038/s41536-021-00127-1, 6:1.

[4] H. Fan, J.P. Gong, Bioinspired underwater adhesives, Adv. Mater. 33 (44) (Nov. 2021), https://doi.org/10.1002/adma.202102983.

[5] P. Frantzis, Durability of adhesive joints made underwater, J. Mater. Civ. Eng. 20 (10) (Oct. 2008) 635–639, https://doi.org/10.1061/(ASCE)0899-1561(2008)20:10(635).

[6] D.G. DeMartini, J.M. Errico, S. Sjoestroem, A. Fenster, J.H. Waite, A cohort of new adhesive proteins identified from transcriptomic analysis of mussel foot glands, J R Soc Interface 14 (131) (Jun. 2017), https://doi.org/10.1098/rsif.2017.0151.

[7] E.W. Danner, Y. Kan, M.U. Hammer, J.N. Israelachvili, J.H. Waite, Adhesion of mussel foot protein mefp-5 to mica: an underwater superglue, Biochemistry 51 (33) (Aug. 2012) 6511–6518, https://doi.org/10.1021/bi3002538.

[8] Q. Lin, D. Gourdon, C. Sun, N. Holten-Andersen, T.H. Anderson, J.H. Waite, J. N. Israelachvili, Adhesion mechanisms of the mussel foot proteins mfp-1 and mfp-3, Proc. Natl. Acad. Sci. 104 (10) (Mar. 2007) 3782–3786, https://doi.org/10.1073/pnas.0607852104.

[9] C. Zhang, B. Wu, Y. Zhou, F. Zhou, W. Liu, Z. Wang, Mussel-inspired hydrogels: from design principles to promising applications, Chem. Soc. Rev. 49 (11) (2020) 3605–3637, https://doi.org/10.1039/C9CS00849G.

[10] Y. Kan, E.W. Danner, J.N. Israelachvili, Y. Chen, J.H. Waite, Boronate complex formation with dopa containing mussel adhesive protein retards pH-induced oxidation and enables adhesion to mica, PLoS One 9 (10) (Oct. 2014) e108869, https://doi.org/10.1371/journal.pone.0108869.

[11] Q. Guo, J. Chen, J. Wang, H. Zeng, J. Yu, Recent progress in synthesis and application of mussel-inspired adhesives, Nanoscale 12 (3) (2020) 1307–1324, https://doi.org/10.1039/C9NR09780E.

[12] Y. Ma, J. Cao, S. Li, L. Wang, Y. Meng, Y. Chen, Nature-inspired wet drug delivery platforms, Small Methods (Jan. 2024), https://doi.org/10.1002/smtd.202301726.

[13] P. Kord Forooshani, B.P. Lee, Recent approaches in designing bioadhesive materials inspired by mussel adhesive protein, J. Polym. Sci. Polym. Chem. 55 (1) (Jan. 2017) 9–33, https://doi.org/10.1002/pola.28368.

[14] G.G. Giobbe, C. Crowley, C. Luni, S. Campinoti, M. Khedr, K. Kretzschmar, M.M. De Santis, E. Zambaiti, F. Michielin, L. Meran, Q. Hu, G. van Son, L. Urbani, A. Manfredi, M. Giomo, S. Eaton, D. Cacchiarelli, V.S.W. Li, H. Clevers, P. Bonfanti, N. Elvassore, P. De Coppi, Extracellular matrix hydrogel derived from decellularized tissues enables endodermal organoid culture, Nat. Commun. 10 (1) (Dec. 2019) 5658, https://doi.org/10.1038/s41467-019-13605-4.

[15] D. Lam, H.A. Enright, J. Cadena, S.K.G. Peters, A.P. Sales, J.J. Osburn, D.A. Soscia, K.S. Kulp, E.K. Wheeler, N.O. Fischer, Tissue-specific extracellular matrix accelerates the formation of neural networks and communities in a neuron-glia co-culture on a multi-electrode array, Sci. Rep. 9 (1) (Mar. 2019) 4159, https://doi.org/10.1038/s41598-019-40128-1.

[16] W.C.W. Chen, Z. Wang, M.A. Missinato, D.W. Park, D.W. Long, H.-J. Liu, X. Zeng, N.A. Yates, K. Kim, Y. Wang, Decellularized zebrafish cardiac extracellular matrix induces mammalian heart regeneration, Sci. Adv. 2 (11) (Nov. 2016) e1600844, https://doi.org/10.1126/sciadv.1600844.

[17] X. Wang, S. Senapati, A. Akinbote, B. Gnanasambandam, P.S.-H. Park, S.E. Senyo, Microenvironment stiffness requires decellularized cardiac extracellular matrix to promote heart regeneration in the neonatal mouse heart, Acta Biomater. 113 (Sep. 2020) 380–392, https://doi.org/10.1016/j.actbio.2020.06.032.

[18] K.H. Hussein, K.M. Park, L. Yu, H.H. Kwak, H.M. Woo, Decellularized hepatic extracellular matrix hydrogel attenuates hepatic stellate cell activation and liver fibrosis, Mater. Sci. Eng. C 116 (Nov. 2020) 111160, https://doi.org/10.1016/J.MSEC.2020.111160.

[19] S.B. Seif-Naraghi, J.M. Singelyn, M.A. Salvatore, K.G. Osborn, J.J. Wang, U. Sampat, O.L. Kwan, G.M. Strachan, J. Wong, P.J. Schup-Magoffin, R.L. Braden, K. Bartels, J.A. DeQuach, M. Preul, A.M. Kinsey, A.N. DeMaria, N. Dib, K. L. Christman, Safety and efficacy of an injectable extracellular matrix hydrogel for treating myocardial infarction, Sci. Transl. Med. 5 (173) (Feb. 2013) 173ra25, https://doi.org/10.1126/scitranslmed.3005503.

[20] X. Wang, V. Pierre, C. Liu, S. Senapati, P.S.-H. Park, S.E. Senyo, Exogenous extracellular matrix proteins decrease cardiac fibroblast activation in stiffening microenvironment through CAPG, J. Mol. Cell. Cardiol. 159 (Oct. 2021) 105–119, https://doi.org/10.1016/j.yjmcc.2021.06.001.

[21] X. Wang, H. Shi, S. Huang, Y. Zhang, X. He, Q. Long, B. Qian, Y. Zhong, Z. Qi, Q. Zhao, X. Ye, Localized delivery of anti-inflammatory agents using extracellular matrix-nanostructured lipid carriers hydrogel promotes cardiac repair post-myocardial infarction, Biomaterials 302 (Nov. 2023) 122364, https://doi.org/10.1016/j.biomaterials.2023.122364.

[22] X. Wang, A. Ansari, V. Pierre, K. Young, C.R. Kothapalli, H.A. von Recum, S. E. Senyo, Injectable extracellular matrix microparticles promote heart regeneration in mice with post-ischemic heart injury, Adv Healthc Mater 11 (8) (Apr. 2022) 2102265, https://doi.org/10.1002/adhm.202102265.

[23] Marcos Luciano Bruschi, Strategies to Modify the Drug Release from Pharmaceutical Systems, Elsevier, 2015, https://doi.org/10.1016/C2014-0-02342-8.

[24] D. Hawthorne, A. Pannala, S. Sandeman, A. Lloyd, Sustained and targeted delivery of hydrophilic drug compounds: a review of existing and novel technologies from bench to bedside, J. Drug Deliv. Sci. Technol. 78 (Dec. 2022) 103936, https://doi.org/10.1016/J.JDDST.2022.103936.

[25] National Research Council (US), Committee for the update of the guide for the Care and use of laboratory animals. Guide for the Care and Use of Laboratory Animals, eighth ed., National Academies Press (US), 2011 https://doi.org/10.17226/12910.

[26] M. Yampolsky, I. Bachelet, Y. Fuchs, Reproducible strategy for excisional skin-wound-healing studies in mice, Nat. Protoc. 19 (1) (Jan. 2024) 184–206, https://doi.org/10.1038/s41596-023-00899-4.

[27] L. Dunn, H.C.G. Prosser, J.T.M. Tan, L.Z. Vanags, M.K.C. Ng, C.A. Bursill, Murine model of wound healing, JoVE J. (75) (May 2013), https://doi.org/10.3791/50265.

[28] C. Hu, G. Chiang, A.H.-P. Chan, C. Alcazar, K.H. Nakayama, M. Quarta, T.A. Rando, N.F. Huang, A mouse model of volumetric muscle loss and therapeutic scaffold implantation, Nat. Protoc. 20 (3) (Mar. 2025) 608–619, https://doi.org/10.1038/s41596-024-01059-y.

[29] S. Chen, Y. Zhou, Y. Chen, J. Gu, fastp: an ultra-fast all-in-one FASTQ preprocessor, Bioinformatics 34 (17) (Sep. 2018) i884–i890, https://doi.org/10.1093/bioinformatics/bty560.

[30] D. Kim, B. Langmead, S.L. Salzberg, HISAT: a fast spliced aligner with low memory requirements, Nat. Methods 12 (4) (2015) 357–360, https://doi.org/10.1038/nmeth.3317. Mar. 2015.

[31] M.I. Love, W. Huber, S. Anders, Moderated estimation of fold change and dispersion for RNA-seq data with DESeq2, Genome Biol. 15 (12) (Dec. 2014) 550, https://doi.org/10.1186/s13059-014-0550-8.

[32] S. Carbon, E. Douglass, B.M. Good, D.R. Unni, N.L. Harris, C.J. Mungall, S. Basu, R. L. Chisholm, J. Elser, et al., The Gene Ontology resource: enriching a GOld mine, Nucleic Acids Res. 49 (D1) (Jan. 2021) D325–D334, https://doi.org/10.1093/NAR/GKAA1113.
[33] M. Kanehisa, M. Furumichi, Y. Sato, M. Kawashima, M. Ishiguro-Watanabe, KEGG for taxonomy-based analysis of pathways and genomes, Nucleic Acids Res. 51 (D1) (Jan. 2023) D587–D592, https://doi.org/10.1093/NAR/GKAC963.
[34] M. Gillespie, B. Jassal, R. Stephan, M. Milacic, K. Rothfels, A. Senff-Ribeiro, J. Griss, C. Sevilla, L. Matthews, C. Gong, C. Deng, T. Varusai, E. Ragueneau, Y. Haider, B. May, V. Shamovsky, J. Weiser, T. Brunson, N. Sanati, L. Beckman, X. Shao, A. Fabregat, K. Sidiropoulos, J. Murillo, G. Viteri, J. Cook, S. Shorser, G. Bader, E. Demir, C. Sander, R. Haw, G. Wu, L. Stein, H. Hermjakob, P. D'Eustachio, The reactome pathway knowledgebase 2022, Nucleic Acids Res. 50 (D1) (Jan. 2022) D687–D692, https://doi.org/10.1093/NAR/GKAB1028.
[35] M. Martens, A. Ammar, A. Riutta, A. Waagmeester, D.N. Slenter, K. Hanspers, R. A. Miller, D. Digles, E.N. Lopes, F. Ehrhart, L.J. Dupuis, L.A. Winckers, S.L. Coort, E.L. Willighagen, C.T. Evelo, A.R. Pico, M. Kutmon, WikiPathways: connecting communities, Nucleic Acids Res. 49 (D1) (Jan. 2021) D613–D621, https://doi.org/10.1093/NAR/GKAA1024.
[36] A. Subramanian, P. Tamayo, V.K. Mootha, S. Mukherjee, B.L. Ebert, M.A. Gillette, A. Paulovich, S.L. Pomeroy, T.R. Golub, E.S. Lander, J.P. Mesirov, Gene set enrichment analysis: a knowledge-based approach for interpreting genome-wide expression profiles, Proc. Natl. Acad. Sci. 102 (43) (Oct. 2005) 15545–15550, https://doi.org/10.1073/pnas.0506580102.
[37] A. Cihanoğlu, J.D. Schiffman, S.A. Altinkaya, Ultrasound-assisted dopamine polymerization: rapid and oxidizing agent-free polydopamine coatings on membrane surfaces, Chem. Commun. 57 (100) (2021) 13740–13743, https://doi.org/10.1039/D1CC05960B.
[38] Y. Liu, K. Ai, L. Lu, Polydopamine and its derivative materials: synthesis and promising applications in energy, environmental, and biomedical fields, Chem Rev 114 (9) (May 2014) 5057–5115, https://doi.org/10.1021/cr400407a.
[39] B. Feng, T. Ji, X. Wang, W. Fu, L. Ye, H. Zhang, F. Li, Engineering cartilage tissue based on cartilage-derived extracellular matrix cECM/PCL hybrid nanofibrous scaffold, Mater. Des. 193 (Aug. 2020) 108773, https://doi.org/10.1016/j.matdes.2020.108773.
[40] R. Raj, T. V Anilkumar, A. Rajan, Preparation and characterization of cholecystic extracellular matrix powder forms for biomedical applications, Biomed Phys Eng Express 4 (4) (Jul. 2018) 047008, https://doi.org/10.1088/2057-1976/aacf59.
[41] Y. Fu, W.J. Kao, Drug release kinetics and transport mechanisms of non-degradable and degradable polymeric delivery systems, Expert Opin Drug Deliv 7 (4) (Apr. 2010) 429–444, https://doi.org/10.1517/17425241003602259.
[42] R.J. Oaks, R. Cindass, Silver sulfadiazine, in: StatPearls [Internet], StatPearls Publishing, Treasure Island (FL), 2024.
[43] F.W. Fuller, The side effects of silver sulfadiazine, J. Burn Care Res. 30 (3) (May 2009) 464–470, https://doi.org/10.1097/BCR.0b013e3181a28c9b.
[44] T. Lagziel, M. Asif, L. Born, L.H. Quiroga, E. Duraes, B. Slavin, P. Shetty, J. Caffrey, C.S. Hultman, Evaluating the efficacy, safety, and tolerance of silver sulfadiazine dressings once daily versus twice daily in the treatment of burn wounds, J. Burn Care Res. 42 (6) (Nov. 2021) 1136–1139, https://doi.org/10.1093/JBCR/IRAB141.
[45] S.S. Mathew-Steiner, S. Roy, C.K. Sen, Collagen in wound healing, Bioengineering 8 (5) (May 2021) 63, https://doi.org/10.3390/bioengineering8050063.
[46] E. Conde-Montero, P. de la Cueva Dobao, J.M. Martínez González, Platelet-rich plasma for the treatment of chronic wounds: evidence to date, Chron. Wound Care Manag. Res. 4 (Sep. 2017) 107–120, https://doi.org/10.2147/CWCMR.S118655.
[47] R. Verma, S. Kumar, P. Garg, Y.K. Verma, Platelet-rich plasma: a comparative and economical therapy for wound healing and tissue regeneration, Cell Tissue Bank. 24 (2) (Jun. 2023) 285–306, https://doi.org/10.1007/s10561-022-10039-z.
[48] Q. Chen, Y. Chen, Y. Zhang, L. Zhang, K. Chen, Z. He, C. Wang, L. Yu, Prognostic impact of platelet-large cell ratio in myelodysplastic syndromes, Front. Oncol. 12 (Apr) (2022), https://doi.org/10.3389/fonc.2022.846044.
[49] M. Gawlita, J. Wasilewski, T. Osadnik, R. Reguła, K. Bujak, M. Gonera, Mean platelet volume and platelet-large cell ratio as prognostic factors for coronary artery disease and myocardial infarction, Folia Cardiol. 10 (6) (Jan. 2016) 418–422, https://doi.org/10.5603/FC.2015.0079.
[50] M.S. Hu, G.G. Walmsley, L.A. Barnes, K. Weiskopf, R.C. Rennert, D. Duscher, M. Januszyk, Z.N. Maan, W.X. Hong, A.T.M. Cheung, T. Leavitt, C.D. Marshall, R. C. Ransom, S. Malhotra, A.L. Moore, J. Rajadas, H.P. Lorenz, I.L. Weissman, G. C. Gurtner, M.T. Longaker, Delivery of monocyte lineage cells in a biomimetic scaffold enhances tissue repair, JCI Insight 2 (19) (Oct. 2017), https://doi.org/10.1172/jci.insight.96260.
[51] C.E. Olingy, C.L. San Emeterio, M.E. Ogle, J.R. Krieger, A.C. Bruce, D.D. Pfau, B. T. Jordan, S.M. Peirce, E.A. Botchwey, Non-classical monocytes are biased progenitors of wound healing macrophages during soft tissue injury, Sci. Rep. 7 (1) (Mar. 2017) 447, https://doi.org/10.1038/s41598-017-00477-1.
[52] F. Ye, S. Mathur, M. Liu, S.E. Borst, G.A. Walter, H.L. Sweeney, K. Vandenborne, Overexpression of insulin-like growth factor-1 attenuates skeletal muscle damage and accelerates muscle regeneration and functional recovery after disuse, Exp. Physiol. 98 (5) (May 2013) 1038–1052, https://doi.org/10.1113/EXPPHYSIOL.2012.070722.
[53] J.D. Schertzer, G.S. Lynch, Comparative evaluation of IGF-I gene transfer and IGF-I protein administration for enhancing skeletal muscle regeneration after injury, Gene Ther. 13 (23) (Dec. 2006) 1657–1664, https://doi.org/10.1038/sj.gt.3302817.
[54] D. Zhou, S. Li, M. Pei, H. Yang, S. Gu, Y. Tao, D. Ye, Y. Zhou, W. Xu, P. Xiao, Dopamine-modified hyaluronic acid hydrogel adhesives with fast-forming and high tissue adhesion, ACS Appl. Mater. Interfaces 12 (16) (Apr. 2020) 18225–18234, https://doi.org/10.1021/acsami.9b22120.
[55] Y. Wang, Y. Zhang, Y.-P. Yang, M.-Y. Jin, S. Huang, Z.-M. Zhuang, T. Zhang, L.-L. Cao, X.-Y. Lin, J. Chen, Y.-Z. Du, J. Chen, W.-Q. Tan, Versatile dopamine-functionalized hyaluronic acid-recombinant human collagen hydrogel promoting diabetic wound healing via inflammation control and vascularization tissue regeneration, Bioact. Mater. 35 (May 2024) 330–345, https://doi.org/10.1016/j.bioactmat.2024.02.010.
[56] S. Jiang, Y. Zhuang, M. Cai, X. Wang, K. Lin, Decellularized extracellular matrix: a promising strategy for skin repair and regeneration, Engineered Regeneration 4 (4) (Dec. 2023) 357–374, https://doi.org/10.1016/j.engreg.2023.05.001.
[57] G.S. Hussey, J.L. Dziki, S.F. Badylak, Extracellular matrix-based materials for regenerative medicine, Nat. Rev. Mater. 3 (7) (May 2018) 159–173, https://doi.org/10.1038/s41578-018-0023-x.
[58] T.C. Ezike, U.S. Okpala, U.L. Onoja, C.P. Nwike, E.C. Ezeako, O.J. Okpara, C. C. Okoroafor, S.C. Eze, O.L. Kalu, E.C. Odoh, U.G. Nwadike, J.O. Ogbodo, B. U. Umeh, E.C. Ossai, B.C. Nwanguma, Advances in drug delivery systems, challenges and future directions, Heliyon 9 (6) (Jun. 2023) e17488, https://doi.org/10.1016/j.heliyon.2023.e17488.
[59] S. Fanse, Q. Bao, Y. Zou, Y. Wang, D.J. Burgess, Impact of polymer crosslinking on release mechanisms from long-acting levonorgestrel intrauterine systems, Int J Pharm 612 (Jan. 2022) 121383, https://doi.org/10.1016/j.ijpharm.2021.121383.
[60] S. Khan, N.M. Ranjha, Effect of degree of cross-linking on swelling and on drug release of low viscous chitosan/poly(vinyl alcohol) hydrogels, Polym. Bull. 71 (8) (Aug. 2014) 2133–2158, https://doi.org/10.1007/s00289-014-1178-2.
[61] H.-W. Sung, R.-N. Huang, L.L.H. Huang, C.-C. Tsai, In vitro evaluation of cytotoxicity of a naturally occurring cross-linking reagent for biological tissue fixation, J. Biomater. Sci. Polym. Ed. 10 (1) (Jan. 1999) 63–78, https://doi.org/10.1163/156856299X00289.
[62] C. Williams, K.P. Quinn, I. Georgakoudi, L.D. Black, Young developmental age cardiac extracellular matrix promotes the expansion of neonatal cardiomyocytes in vitro, Acta Biomater. 10 (1) (Jan. 2014) 194–204, https://doi.org/10.1016/J.ACTBIO.2013.08.037.
[63] Z. Wang, D.W. Long, Y. Huang, W.C.W. Chen, K. Kim, Y. Wang, Decellularized neonatal cardiac extracellular matrix prevents widespread ventricular remodeling in adult mammals after myocardial infarction, Acta Biomater. 87 (Mar. 2019) 140–151, https://doi.org/10.1016/j.actbio.2019.01.062.
[64] V.Z. Beachley, M.T. Wolf, K. Sadtler, S.S. Manda, H. Jacobs, M.R. Blatchley, J. S. Bader, A. Pandey, D. Pardoll, J.H. Elisseeff, Tissue matrix arrays for high-throughput screening and systems analysis of cell function, Nat. Methods 12 (12) (Dec. 2015) 1197–1204, https://doi.org/10.1038/nmeth.3619.
[65] J.H. Traverse, T.D. Henry, N. Dib, A.N. Patel, C. Pepine, G.L. Schaer, J.A. DeQuach, A.M. Kinsey, P. Chamberlin, K.L. Christman, First-in-Man study of a cardiac extracellular matrix hydrogel in early and late myocardial infarction patients, JACC Basic Transl Sci 4 (6) (Oct. 2019) 659–669, https://doi.org/10.1016/j.jacbts.2019.07.012.
[66] S. Sahoo, T. Kariya, K. Ishikawa, Targeted delivery of therapeutic agents to the heart, Nature Reviews Cardiology 2021 18 (6) (Jan. 2021) 389–399, https://doi.org/10.1038/s41569-020-00499-9, 18:6.
[67] J. Dziki, S. Badylak, M. Yabroudi, B. Sicari, F. Ambrosio, K. Stearns, N. Turner, A. Wyse, M.L. Boninger, E.H.P. Brown, J.P. Rubin, An acellular biologic scaffold treatment for volumetric muscle loss: results of a 13-patient cohort study, NPJ Regen. Med. 1 (1) (Jul. 2016) 16008, https://doi.org/10.1038/npjregenmed.2016.8.
[68] W. Lee, J.Y. Lee, H.S. Lee, Y. Yoo, H. Shin, H. Kim, D.S. Min, J.S. Bae, Y.K. Seo, Thermosensitive hydrogel harboring CD146/IGF-1 nanoparticles for skeletal-muscle regeneration, ACS Appl. Bio Mater. 4 (9) (Sep. 2021) 7070–7080, https://doi.org/10.1021/ACSABM.1C00688/ASSET/IMAGES/LARGE/MT1C00688_0005.JPEG.
[69] T. Yoshida, P. Delafontaine, Mechanisms of IGF-1-mediated regulation of skeletal muscle hypertrophy and atrophy, Cells 9 (9) (Aug. 2020) 1970, https://doi.org/10.3390/CELLS9091970.
[70] J. Zhang, J. Muri, G. Fitzgerald, S.-A. Iz, M. Kopf, K. De Bock, Endothelial lactate controls muscle regeneration from ischemia by inducing M2-like macrophage polarization, Cell Metab. 31 (2020) 1136–1153.e7, https://doi.org/10.1016/j.cmet.2020.05.004.
[71] T.M. Raimondo, D.J. Mooney, Functional muscle recovery with nanoparticle-directed M2 macrophage polarization in mice, Proc. Natl. Acad. Sci. U. S. A. 115 (42) (Oct. 2018) 10648–10653, https://doi.org/10.1073/PNAS.1806908115/SUPPL_FILE/PNAS.1806908115.SAPP.PDF.